The Step-Mountain, Eta Coordinate Regional Model:

A Documentation

Thomas L. Black

Development Division
National Meteorological Center

April 1988

Table of Contents

1. Introduction

The use of the sigma coordinate (Phillips, 1957) is widely accepted in describing vertical space in models of the atmosphere since it precludes the intersection of predictive surfaces with the ground. However, the steep slopes of sigma coordinate surfaces over mountainous terrain presents another problem, namely the potentially less accurate calculation of the pressure gradient force since in such regions it is often equal to the sum of two large, opposing terms. Difficulties also arise in calculations of the horizontal advection and diffusion terms. Several remedies have been suggested (e.g. Phillips, 1974; Janjić, 1977; Johnson and Uccellini, 1983).

In order to directly eliminate the problem of steep slopes while retaining the simplicity of a terrain-following system, Mesinger (1984) proposed the eta coordinate for use in conjunction with step-like terrain. Mesinger, et al., (1988) describe early results from a regional forecast model based upon the eta system but which included no physical parameterizations. A comprehensive physical package was subsequently incorporated. A complete description of the entire model will now be presented.

2 Model Characteristics

2.1 The Horizontal Grid

The semi-staggered E grid (Winninghoff, 1968; Arakawa and Lamb, 1977) is used in the eta model to describe horizontal space. It has been clearly demonstrated that grids A and D are undesirable due to large errors in describing wave amplitudes and phase and group velocities. In simulating the geostrophic adjustment process, the C grid displays significant errors for higher internal modes at all wavelengths. While the B and E grids show a grid separation problem at short wavelengths, a method which largely eliminates this problem has been developed (Mesinger, 1973; Janjic, 1979) and will be described in Section 3.2. Horizontal advection schemes have been developed for both the C and E grids which control energy cascade to smaller scales (Arakawa and Lamb, 1981; Janjic, 1984). In the case of the C grid, potential enstrophy is conserved. On the E grid, momentum is conserved and the false energy cascade toward the $2\Delta x$ wavelength within the nondivergent part of the flow is completely prevented. Lastly it appears that the linear amplitude response to forcing by topography in the B and E grid schemes may be more accurate than that of the C grid schemes (Dragosavac and Janjic, 1987). Collectively these considerations led to the choice of the E grid.

A sample of the grid as used in the eta model is depicted in Fig. 1 accompanied by the two sets of axes. The x and y axes are oriented east and north, respectively, while the primed axes are rotated 45° counterclockwise. As will be seen in subsequent sections, proper attention must be given to differencing and averaging in all four directions to ensure conservation of important quantities.

The grid points are aligned along parallels and meridians of latitude and longitude. On a standard lat-lon grid, the shrinking of Δx with respect to Δy as one moves poleward is undesirable. In the eta model, the coordinates are transformed by placing the new equator through the center of the region of interest thereby ensuring that the grid boxes will be less elongated in that region. For a given region size and resolution this maximizes the smallest value of Δx thereby increasing the efficiency of the model. Let (ϕ,λ) represent the geodetic latitude and longitude of a point and (Φ,Λ) represent the transformed latitude and longitude. At the grid point in the center of the domain $\phi=\phi_0$, $\lambda=\lambda_0$, $\Phi=0$, $\Lambda=0$. If the standard convention of north latitude and west longitude as positive is used for the geodetic values, while east longitude is positive in the model,

$$\Phi = \tan^{-1}\left(\frac{Z}{\sqrt{(X^2+Y^2)}}\right)$$

$$\Lambda = \tan^{-1}\left(\frac{Y}{X}\right)$$

$$X = \cos\phi_0\cos\phi\cos(\lambda-\lambda_0)+\sin\phi_0\sin\phi \qquad (1)$$

$$Y = -\cos\phi \sin(\lambda - \lambda_0)$$

$$Z = -\sin\phi_0 \cos\phi \cos(\lambda - \lambda_0) + \cos\phi_0 \sin\phi$$

To convert from transformed to geodetic coordinates, the following relations hold:

$$\phi = \sin^{-1}(\sin\Phi\cos\phi_0 + \cos\Phi\sin\phi_0\cos\Lambda) \qquad (2a)$$

$$\lambda = \lambda_0 \pm \cos^{-1}\left(\frac{\cos\Phi\cos\Lambda}{\cos\phi\cos\phi_0} - \tan\phi\tan\phi_0\right) \qquad (2b)$$

where the + is used in (2b) for $\Lambda<0$ and the - for $\Lambda>0$.

Note that transforming the coordinates introduces no added complexities except that the Coriolis parameter will be a function of both latitude and longitude. The increments currently used for the model's standard resolution are

$$\Delta\Phi = (14/26)^\circ \text{ and } \Delta\Lambda = (15/26)^\circ$$

yielding a grid resolution (the quantity 'd' in Fig. 1) ranging from 79.6 km at the southern and northern boundaries to 87.7 km at the center. The domain is defined to cover 70° x 75° of transformed latitude by longitude with the center located at geodetic coordinates 52.5° N and 100° W.

2.2 The Eta Coordinate and Vertical Grid

The value of eta is defined by

$$\eta = \sigma\eta_s \qquad (3a)$$

where

$$\eta_s = \frac{p_{ref}(z_{sfc}) - p_T}{p_{ref}(0) - p_T} \qquad (3b)$$

and

$$\sigma = \frac{p - p_T}{p_{sfc} - p_T} \; . \qquad (3c)$$

Here z_{sfc} and p_{sfc} are the height and pressure at the surface of the model terrain, p_T is the constant pressure at the top of the domain (10^4 Pa), and p_{ref} is a reference pressure state independent of time for which the standard atmosphere is currently used. Defined as such, the eta surfaces are always nearly horizontal. It can be seen from Eqs. (3a) and (3b) that η is nothing more than a generalization of σ. This means that the predictive equations are essentially the same as in sigma coordinates except for the inclusion of η_s. When η_s is set to 1, η becomes σ precisely, thereby easily allowing comparisons between the two systems.

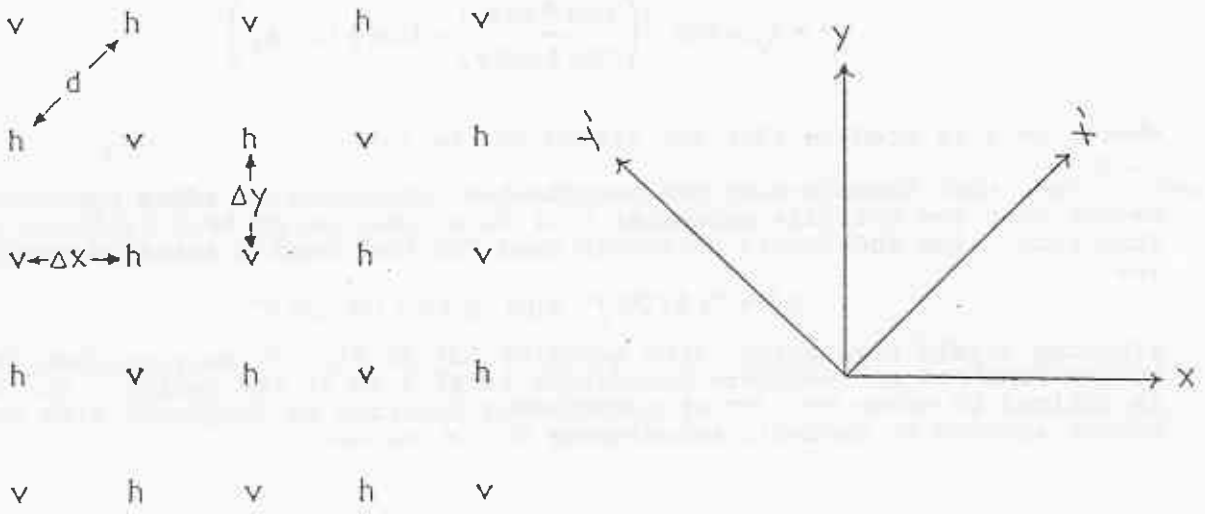

Fig. 1. (Left) The semi-staggered E grid; (right) the coordinate axes.

There are currently sixteen (LMAX) predictive levels in the model with vertical resolution highest near the bottom and top of the domain. ~~Because the equations are in flux form,~~ the predictive levels carry values representing layers which are separated by interfacial levels where heights are stored. The model terrain is constructed so as to "fill" layers to the interfacial levels. A vertical cross section of the domain is shown in Fig. 2. Note that temperature (T) and specific humidity (q) are specified at those points designated for height in Fig. 1. Wind components at the steps (circled in Fig. 2) like those underground are identically zero.

Values for $\Delta\eta$ are as follows, with level 1 at the top of the domain:

Layer Index	$\Delta\eta$
L=1	0.053813
L=2	0.060517
L=3	0.065860
L=4	0.069920
L=5	0.072710
L=6	0.074320
L=7	0.074770
L=8	0.074110
L=9	0.072420
L=10	0.069710
L=11	0.066070
L=12	0.061510
L=13	0.056110
L=14	0.049910
L=15	0.042950
L=16	0.035300

Having chosen the vertical resolution, reference heights of the layer interfaces are calculated by integrating the hypsometric equation with the chosen reference atmosphere. These heights will be used in determining the topography.

2.3 Indexing

Fig. 3 indicates how the grid points are ordered for array storage. IM and JM are the number of increments in each direction. Each "cell" contains one height point and one velocity point. A consequence of this is the grouping of velocity points on the left boundary with height points that are on the right boundary and are one row lower. These velocities are starred in Fig. 3. Now the two-dimensional grid can be ordered in a one-dimensional fashion as given by the K index in order to expedite vectorization.

With the exception of convection, most calulations are carried out sequentially on each eta level looping through the K index as a single vector. Because the presence of steps on a given level would seem to eliminate the possibility of vectorization, an auxilliary three-dimensional array exists which holds values of 1 for all points above ground and 0 for all points below. Similarly because the outer two rows around the domain are excluded from direct integration, a two-dimensional array consisting of 0 in these rows and 1 elsewhere is carried. Multiplying the equations by these topography and boundary masks completely resolves the problem of vectorization through the steps and outside the integration domain.

~~The angle of rotation (α) needed to rotate wind components from the transformed coordinates~~

The following formulae may be used to rotate wind components from transformed to geodetic coordinates:

$$u_g = u_m \cos\alpha + v_m \sin\alpha$$

$$v_g = v_m \cos\alpha - u_m \sin\alpha$$

where

$$\alpha = \sin^{-1}\left[\frac{\sin\phi_0 \sin\Lambda}{\cos\phi}\right]$$

and the subscript 'g' denotes the geodetic system.

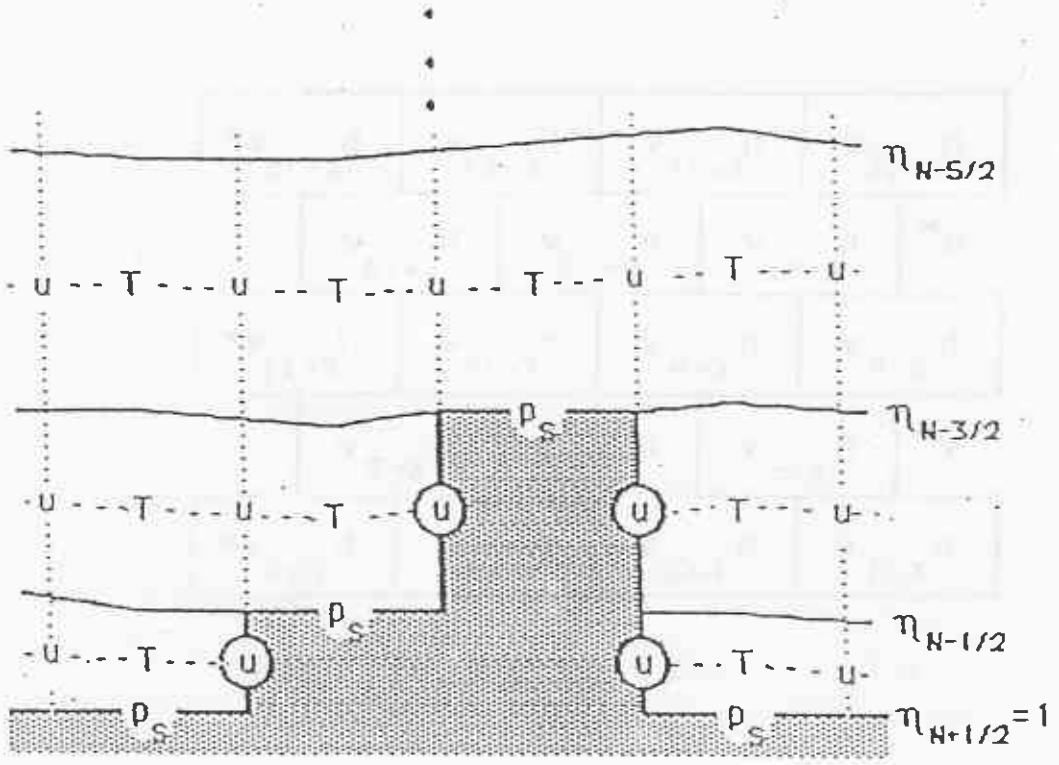

Fig. 2. Vertical cross section of the eta model domain with step topography.

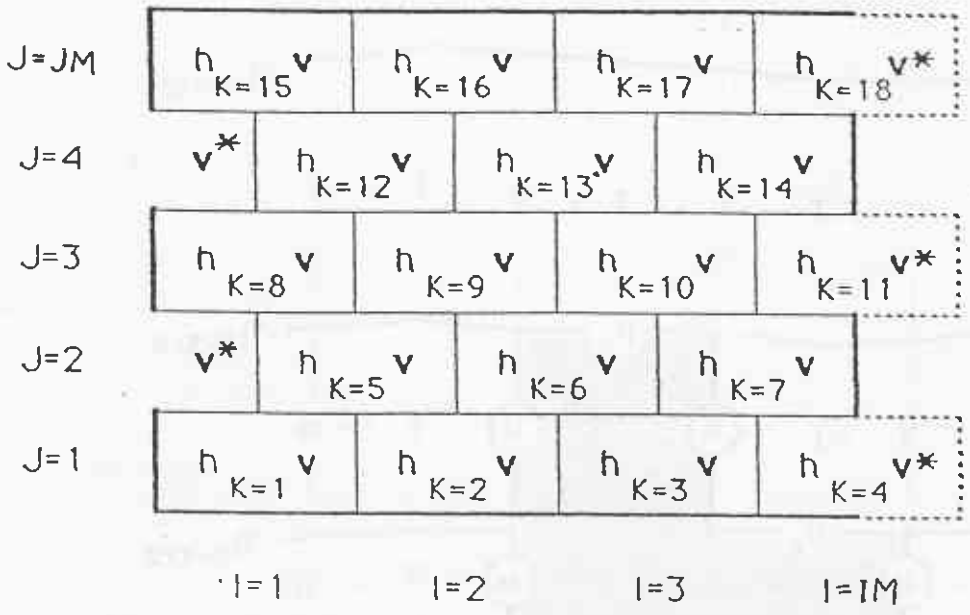

Fig. 3. Depiction of the E grid showing relationship between two-dimensional (I,J) and one-dimensional (K) indexing.

2.4 Specification of Topography and Initial Data

The elevation of each step mountain is arrived at through a method for describing enhanced "silhouette" topography. Equal values are assigned to groups of four neighboring height points to avoid the possibility of having a single height point surrounded on all sides by mountains.

Consider Fig. 4 which shows a group of four adjacent height points. Note that each of the grid squares is divided into four sub-boxes. Actual surface elevations are read from archived data and the mean is found within each sub-box. These means are represented by the Z's in Fig. 4. Now eight intermediate quantities are determined by taking the maximum elevation along each row and column of sub-boxes. Specifically,

$$\begin{aligned} S1&=\max(Z1,Z2,Z3,Z4)\\ S2&=\max(Z5,Z6,Z7,Z8)\\ S3&=\max(Z9,Z10,Z11,Z12)\\ S4&=\max(Z13,Z14,Z15,Z16)\\ S5&=\max(Z1,Z5,Z9,Z13)\\ S6&=\max(Z2,Z6,Z10,Z14)\\ S7&=\max(Z3,Z7,Z11,Z15)\\ S8&=\max(Z4,Z8,Z12,Z16) \end{aligned} \qquad (4)$$

The height of the step is simply the mean of these eight values. The archived data includes information of areal coverage of the water surface which is necessary for specifying coastal points. The percentage of water surface in each sub-box is found by summing the amounts for each archive data square within that box and the mean percentage is obtained for all sixteen sub-boxes. If less than 50% of the entire step is covered by water, that step is considered to be land and its elevation is that given above. If more than 50% of the step is covered by water then those four adjacent points are defined as ocean or lake. The surface elevation of the water points ("sea" points in the code) is the mean of the values at the 16 sub-boxes. To avoid special coding that would otherwise be needed near the lateral boundaries, all points are defined as ocean in the outer ~~five~~ four rows.

The final height of the model steps is taken to be the reference height of the interface that is nearest the previously defined elevation at each height point. If this procedure has closed major mountain gaps at saddle points that existed before discretization to reference heights then such gaps are restored. The function η_s (Eq.(3b)) can now be determined and will remain unchanged throughout the model integration since it depends only on the reference atmosphere and the topography.

The initial conditions in the eta model are based on the initialialized fields from the Regional Analysis and Forecast System (RAFS) which are on either mandatory pressure levels or the Nested Grid Model's sigma levels. Interpolation of height values from a pressure level h_p to the eta surfaces h_η is done quadratically in $\ln(p)$, i.e.,

$$A\ln(p)^2 + B\ln(p) + C = h_p \qquad (5)$$

Eq. (5) is applied at three adjacent input pressure levels which are nearest the model ~~topography~~. These three equations are solved simultaneously for A, B, and C. The model terrain height is then inserted into (5) to find the surface pressure.

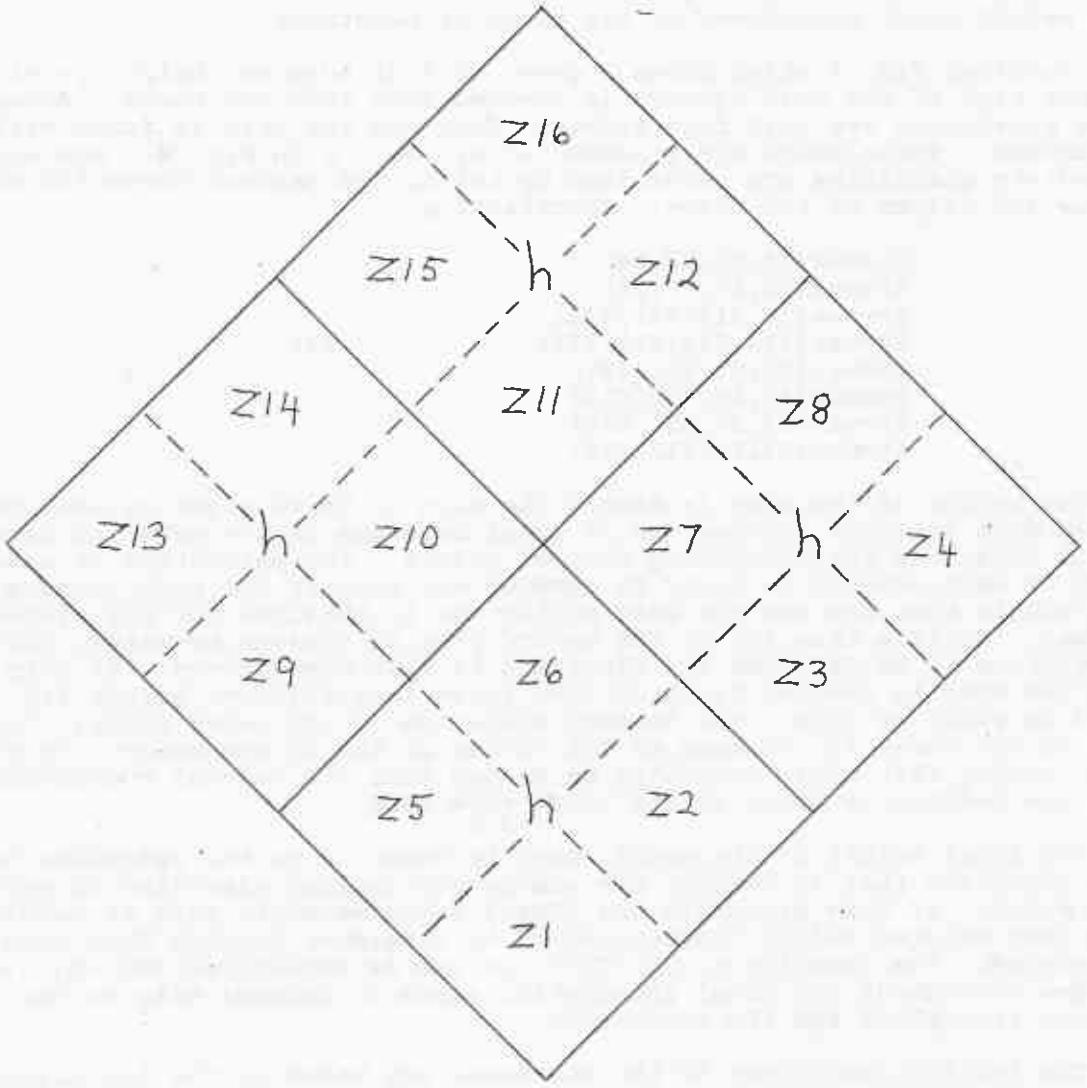

Fig. 4. Surface of one step consisting of four height boxes and sixteen sub-boxes used to calculate the elevation of the step.

To determine the heights of each interfacial eta level (solid surfaces in Fig. 2), A, B, and C are found from three adjacent input pressure levels around each given eta level. The difference of (5) at the middle pressure level from (5) on the eta surface readily yields the desired height:

$$h_\eta = h_{p_2} + A\left\{\ln(p_\eta)^2 - \ln(p_2)^2\right\} + B\left\{\ln(p_\eta) - \ln(p_2)\right\} \qquad (6)$$

where p_2 is the middle of the three input pressure levels. Given the heights at all eta levels, the temperature at each midlayer point is found from the finite-difference form of the hypsometric equation. Initial specific humidities at the midlayer points are determined in a manner analogous to that used for the heights.

The winds at each midlayer velocity point are obtained through linear interpolation in $\ln(p)$. Letting p_L be the input pressure level immediately below the desired eta level, then:

$$u_\eta = u_{p_L} + \left(u_{p_{L-1}} - u_{p_L}\right)\left\{\frac{\ln(p_L) - \ln(p_\eta)}{\ln(p_L) - \ln(p_{L-1})}\right\} \qquad (7)$$

and similarly for v.

See Section 5 for specification of the boundary values.

The sea surface temperature (SST) and snow/ice cover (SI) are taken from the initial guess file. SST's remain constant throughout the forecast. The snow cover is initially given as either present (1) or absent (0) so an actual depth must be assigned arbitrarily. The formula used on land points is

$$SI_{new} = 3\ \left(SI_{old}\right)\ \sin\phi \qquad (8)$$

where ϕ is the geodetic latitude. The snow depth thus varies with latitiude to a maximum of 3 m at the pole. Over sea points, the ice depth is set to 1 m. The values of the "underground potential temperature" (TG) are also constant in time and are given by

$$TG = 258.15 + 30\ \cos\phi + g z_{sfc}/3333. \qquad (9)$$

and thus varies from 288.15K to 258.15K between the equator and the pole with a modification for terrain height. The soil moisture is taken from a global monthly climatology file and a maximum of 0.1125 m is imposed. Initial albedo is read from a global seasonal climatology file.

3 Numerical Methods

3.1 Model Variables and Predictive Equations

The fundamental quantities predicted are the difference between surface pressure and that at the top of the domain (PD), temperature (T), specific humidity (q), and the u and v components of the wind. A sixth, three-dimensional field, the turbulent kinetic energy (Q2), is also predicted for use in the turbulent exchange routines described in Section 4.1. Other evolving fields associated with the surface include accumulated precipitation, soil moisture, albedo, and surface potential temperature.

The complete set of prognostic equations for the fundamental variables is as follows:

$$\frac{\partial}{\partial t}\left(\frac{\partial p}{\partial \eta}\vec{V}\right)+\nabla_\eta\cdot\left(\frac{\partial p}{\partial \eta}\vec{V}\vec{V}\right)+\frac{\partial}{\partial \eta}\left(\frac{\partial p}{\partial \eta}\dot{\eta}\vec{V}\right)+$$

$$\left(\frac{\partial p}{\partial \eta}\right)\left(f\vec{k}\times\vec{V}+\nabla_\eta\phi+\frac{R_d T_v}{p}\nabla_\eta p+\vec{F}\right)=0 \qquad (10a)$$

$$\frac{dT}{dt}-\frac{\kappa T\omega}{p}+T'+\frac{g}{c_p}\frac{\partial R}{\partial \eta}\Big/\frac{\partial p}{\partial \eta}=0 \qquad (10b)$$

$$\frac{\partial \phi}{\partial \eta}=\frac{-R_d T_v}{p}\frac{\partial p}{\partial \eta} \qquad (10c)$$

$$\frac{1}{\eta_s}\frac{\partial p_{sfc}}{\partial t}+\nabla_\eta\cdot\left(\frac{\partial p}{\partial \eta}\vec{V}\right)+\frac{\partial}{\partial \eta}\left(\frac{\partial p}{\partial \eta}\dot{\eta}\right)=0 \qquad (10d)$$

$$\frac{\partial p_{sfc}}{\partial t}=-\int_0^{\eta_s}\nabla_\eta\cdot\left(\frac{\partial p}{\partial \eta}\vec{V}\right)d\eta \qquad (10e)$$

$$\dot{\eta}\frac{\partial p}{\partial \eta}=-\frac{\eta}{\eta_s}\frac{\partial p_{sfc}}{\partial t}-\int_0^{\eta}\nabla_\eta\cdot\left(\frac{\partial p}{\partial \eta}\vec{V}\right)d\eta \qquad (10f)$$

$$\frac{dq}{dt}+q'=S \qquad (10g)$$

In the equations above,

$\overline{F}$ represents frictional and turbulent effects on the velocity,

ϕ is the geopotential $\kappa = R_d / c_p$

R is the net vertical radiative flux

T' represents turbulent effects on the temperature

q' represents turbulent effects on specific humidity

S represents sources and sinks of water vapor.

The eta model uses the split-explicit approach (Gadd, 1978) in integrating the equations in (10) separating the adjustment processes from the advection. The fundamental time step in the model is that for the adjustment, Δt_{adj}, and currently equals 240 s. Advection and physical processes are calculated at integral multiples of Δt_{adj}.

3.2 Adjustment Stage

In essence, the semi-staggered E grid is a superposition of two staggered C grids. When only the adjustment terms in the equations of motion and continuity are considered it may be shown that two large scale solutions from each C grid may exist independently and a noisy total solution results. When Coriolis and advection terms are included, these gravity wave solutions may interact in a manner that is physically unrealistic. Rather than filter this small scale noise, the eta model employs the forward-backward scheme modified to prevent gravity wave separation in describing the adjustment stage (Mesinger, 1973; Mesinger and Arakawa, 1976; Janjic, 1979). The unmodified forward-backward scheme is illustrated in the following difference equations:

$$u^{n+1} = u^n - \Delta t_{adj} P_x^{n+1} \qquad (11a)$$

$$v^{n+1} = v^n - \Delta t_{adj} P_y^{n+1} \qquad (11b)$$

$$PD^{n+1} = PD^n - \left\{ \sum_{L=1}^{LM} \nabla_\eta \cdot \frac{\partial p}{\partial \eta} \vec{V} \Delta\eta \right\}^n \Delta t_{adj} \qquad (11c)$$

where P_x and P_y are the components of the pressure gradient force and LM is the lowest predictive level above the surface. Note that the mass field is determined using a forward time difference while the velocity components are obtained using a backward time difference. The stability criterion for the scheme allows a doubling of the time step compared to an analogous leapfrog setup and no computational mode is produced.

~~In the adjustment routine, velocity components are determined first which means the pressure gradient is needed~~. The form of the pressure gradient was developed to achieve consistency with the advection scheme of the model (Mesinger and Janjic, 1987) and the components are given by

New values of PD are determined first
en wind components are updated using the
essure gradients of the new mass field.

$$P_x = \frac{-1}{2\Delta x}\{\frac{1}{3}\left[\overline{\delta_x \cdot \phi}^{y\cdot} - \overline{\delta_y \cdot \phi}^{x\cdot} + \overline{(RT/p)^x \delta_x \cdot p}^{y\cdot} - \overline{(RT/p)^y \delta_y \cdot p}^{x\cdot}\right]$$

$$+\frac{2}{3}\frac{1}{\overline{\Delta p}^x}\left[\overline{\Delta p^x \delta_x \cdot \phi}^{y\cdot} - \overline{\Delta p^y \delta_y \cdot \phi}^{x\cdot}\right] \qquad (12a)$$

$$+\frac{2}{3}\frac{1}{\overline{\Delta p}^x}\left[\overline{\Delta p^x (RT/p)^x \delta_x \cdot p}^{y\cdot} - \overline{\Delta p^y (RT/p)^y \delta_y \cdot p}^{x\cdot}\right]\}$$

$$P_y = \frac{-1}{2\Delta y}\{\frac{1}{3}\left[\overline{\delta_x \cdot \phi}^{y\cdot} + \overline{\delta_y \cdot \phi}^{x\cdot} + \overline{(RT/p)^x \delta_x \cdot p}^{y\cdot} + \overline{(RT/p)^y \delta_y \cdot p}^{x\cdot}\right]$$

$$+\frac{2}{3}\frac{1}{\overline{\Delta p}^y}\left[\overline{\Delta p^x \delta_x \cdot \phi}^{y\cdot} + \overline{\Delta p^y \delta_y \cdot \phi}^{x\cdot}\right] \qquad (12b)$$

$$+\frac{2}{3}\frac{1}{\overline{\Delta p}^y}\left[\overline{\Delta p^x (RT/p)^x \delta_x \cdot p}^{y\cdot} + \overline{\Delta p^y (RT/p)^y \delta_y \cdot p}^{x\cdot}\right]\}$$

where Δp represents the pressure depth of a given eta layer. The overbars indicate two-point averaging in the specified direction while $\delta_{x\cdot}$ and $\delta_{y\cdot}$ denote differencing between adjacent values along the indicated direction. The weights of 1/3 and 2/3 arise from the fact that sides of a grid box are nearer the center than are the vertices. P_x and P_y are defined at velocity points.

The Coriolis and curvature terms, $f = 2\Omega\sin\phi + (u/a)\tan\Phi$, are now added to (11a) and (11b) in an implicit fashion.

$$u^{n+1} = u^n + f^n \Delta t_{adj}\left(v^{n+1} + v^n\right)/2 - \Delta t_{adj} P_x^{n+1} \qquad (13a)$$

$$v^{n+1} = v^n - f^n \Delta t_{adj}\left(u^{n+1} + u^n\right)/2 - \Delta t_{adj} P_y^{n+1} \qquad (13b)$$

Eq. (13b) is now substituted into v^{n+1} in (13a) and Eq. (13a) is substituted into u^{n+1} in (13b). When u^{n+1} and v^{n+1} are isolated, the result is

$$u^{n+1} = \left[u^n\left(1 - F^2\right) + 2Fv^n - F\Delta t_{adj} P_y^{n+1} - \Delta t_{adj} P_x^{n+1}\right]/\left[1 + F^2\right] \qquad (14a)$$

$$v^{n+1} = \left[v^n\left(1 - F^2\right) - 2Fu^n + F\Delta t_{adj} P_x^{n+1} - \Delta t_{adj} P_y^{n+1}\right]/\left[1 + F^2\right] \qquad (14b)$$

where

$$F = .5 f^n \Delta t_{adj}$$

If the auxiliary variables UP and VP are introduced

$$UP = u^n + Fv^n - \Delta t_{adj} P_x^{n+1} \qquad (15a)$$

$$VP = v^n - Fu^n - \Delta t_{adj} P_y^{n+1} \tag{15b}$$

then (14a) and (14b) may be rewritten

$$u^{n+1} = (F\ VP + UP)/(1 + F^2) \tag{16a}$$

$$v^{n+1} = VP - Fu^{n+1} \tag{16b}$$

These unmodified wind components are used in calculating the divergence. Mass flux along both sets of axes is needed and Fig. 5 shows the relationship between the different velocity components at a velocity point. The u contribution to v′is negative since u>0 produces a component along the -y′axis.

The divergence appearing in the summation in (11c) and defined at each height point is given by

$$DIV = DIV_{corr} + \frac{1}{3}\left(\frac{1}{2\Delta x \Delta y}\right)\left[\delta_x\left(\overline{\Delta p}^{x} u \Delta y\right) + \delta_y\left(\overline{\Delta p}^{y} v \Delta x\right)\right]$$

$$+\frac{2}{3}\left(\frac{1}{2\Delta x \Delta y}\right)\left\{\delta_{x'}\left[\overline{\Delta p}^{x'}\overline{(u\Delta y + v\Delta x)}^{y'}\right] + \delta_{y'}\left[\overline{\Delta p}^{y'}\overline{(-u\Delta y + v\Delta x)}^{x'}\right]\right\} \tag{17}$$

The quantity on the RHS of (17) weighted by 1/3 is the mass flux divergence along the x and y axes while the quantity weighted by 2/3 is the flux divergence along the x′ and y′ axes. Note that mass is conserved in (17) since each term is in the form of an exact differential.

The ~~final~~ term in (17) which suppresses gravity wave noise essentially involves differencing the divergence of the pressure gradient force at each height point. Let

$P_{x'} = \delta_{x'}\phi + \overline{(RT/p)}^{x'}\delta_{x'}p$ and $P_{y'} = \delta_{y'}\phi + \overline{(RT/p)}^{y'}\delta_{y'}p$.

If, $\Pi = \delta_{x'}P_{y'} + \delta_{y'}P_{x'}$ over each velocity point,

then the correction added to (17) is

$$DIV_{corr} = -0.5\rho^*\left(\overline{\Pi}^{x} - \overline{\Pi}^{y}\right) \tag{18}$$

where

$$\rho^* = -\frac{.88w\left[(\Delta x)^2_{\min} + (\Delta y)^2\right]}{4\Delta t_{adj}\Delta x \Delta y} \tag{19}$$

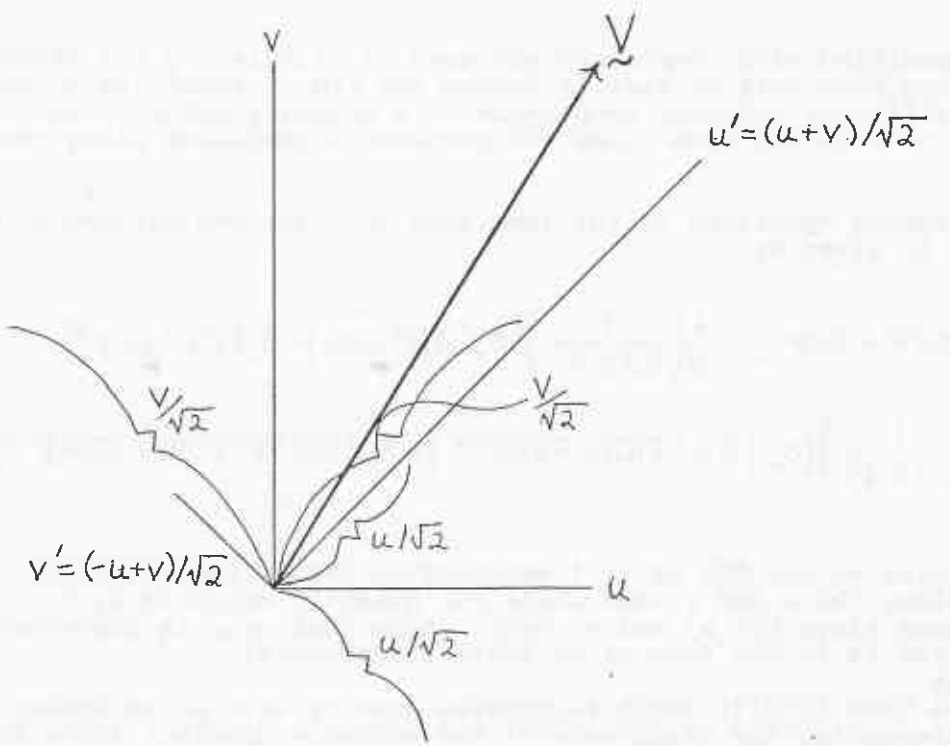

Fig. 5. Relationship between wind vector $\underset{\sim}{V}$ and its components in the x-y and x'-y' directions.

and w=0.25 (see Janjic, 1979) and Δx_{min} is the minimum value of Δx on the grid. The correction term maintains mass conservation since whenever Π is added at a given velocity point in calculating DIV at a given height point, the same Π will be subtracted when an adjacent height point on a different row is considered. To maintain mass conservation with internal boundaries present, values of Π are set equal to zero at all velocity points located at the sides of mountains. Similarly, to conserve mass at the lateral boundaries, Π is set to zero at velocity points along the outermost row of the integration domain (third row from the physical boundary; see Section 5).

After each adjustment time step ~~during the first nine hours of integration~~, the divergent part of the wind is suppressed. Define the variables DDMPU and DDMPV at each velocity point

$$DDMPU = CODAMP \;\; ACDT / \Delta x \tag{20a}$$

$$DDMPV = CODAMP \;\; ACDT / \Delta y \tag{20b}$$

where

$$ACDT = COAC \;\; \Delta t_{adj}\left[\Delta x_{\min}^2 + \Delta y^2\right] \text{ , } CODAMP = 150 \text{ and } COAC = 0.04 \text{ .}$$

The wind is then modified by the relations

$$u_{new} = u_{old} + \left(\delta_x DIV\right) DDMPU / \left(2\overline{\Delta p}^x\right) \tag{21a}$$

$$v_{new} = v_{old} + \left(\delta_y DIV\right) DDMPV / \left(2\overline{\Delta p}^y\right) \tag{21b}$$

Divergence damping is increased near the lateral boundaries by multiplying DDMPU and DDMPV by 8 in the outer five rows of the domain.

A final process described in the adjustment stage is that of adiabatic temperature change associated with the evolving mass field. The second term in (10b) is the so-called $\omega\alpha$ term and involves the substantial derivative of pressure. The tendency of temperature due to the $\omega\alpha$ term may be written as

$$\frac{\partial T}{\partial t} = \frac{1}{c_p}\frac{RT}{p}\left[\vec{V}\cdot\nabla_\eta p - \int_0^\eta \nabla_\eta \cdot \left(\frac{\partial p}{\partial \eta}\vec{V}\right) d\eta\right] \tag{22}$$

where the bracketed quantity is ω.

First the horizontal portion of (22) is computed. Consider the following quantities defined at velocity points:

$$TEW = \overline{\Delta p}^{x} u \Delta y \left[\overline{RT/p}^{x'} \delta_{x'} p^{y'} - \overline{RT/p}^{y'} \delta_{y'} p^{x'} \right] \qquad (23a)$$

$$TNS = \overline{\Delta p}^{y} v \Delta x \left[\overline{RT/p}^{x'} \delta_{x'} p^{y'} + \overline{RT/p}^{y'} \delta_{y'} p^{x'} \right] \qquad (23b)$$

$$TNE = \left[\overline{\Delta p}^{x'} \delta_{x'} p \right] \left[\overline{u \Delta y + v \Delta x}^{y'} \right] \left[\overline{RT/p}^{x'} \right] \qquad (23c)$$

$$TSE = \left[\overline{\Delta p}^{y'} \delta_{y'} p \right] \left[\overline{-u \Delta y + v \Delta x}^{x'} \right] \left[\overline{RT/p}^{y'} \right] \qquad (23d)$$

These represent a flux form of $(RT/p)\vec{V} \cdot \nabla_\eta p$ on the east and west vertices, the north and south vertices, the northeast and southwest sides, and the northwest and southeast sides, respectively, of a grid box. (A grid box will refer to a height point surrounded by four velocity points). The new temperature at each height point on level L is then

$$T^{n+1} = T^{n} + \frac{\Delta t_{adj}}{c_p \Delta x \Delta y \Delta p} \left[\frac{1}{3} \left(\overline{TEW}^{x} + \overline{TNS}^{y} \right) + \frac{2}{3} \left(\overline{TNE}^{x'} + \overline{TSE}^{y'} \right) \right] \qquad (24)$$

For the vertical contribution of (22), consider the quantity SDIV defined as follows:

$$SDIV_{N+\frac{1}{2}} = \sum_{L=1}^{N} \nabla_\eta \cdot \frac{\partial p}{\partial \eta} \vec{V}_L \Delta \eta = \sum_{L=1}^{N} DIV_L \qquad (25)$$

which is simply the sum of the mass flux divergence downward through N eta layers. This integrated value for layer N is valid at the bottom interface of that layer at each height point. When N=LM in (25), the surface pressure tendency in (10e) is obtained. Knowing $\partial p_{sfc}/\partial t$ then $\dot{\eta}$ at the layer interfaces is determined at each height point from (10f) with $\dot{\eta}$ at the top and bottom of the domain equal to zero.

The updated value of temperature at level L due to divergence is

$$T_L^{n+1} = T_L^{n} + 0.5 \left(\Delta t_{adj} / c_p \right) (RT/p) \left[SDIV_{N-\frac{1}{2}} + SDIV_{N+\frac{1}{2}} \right] \qquad (26)$$

This assumes that SDIV at the upper boundary is zero.

3.3 Advection Stage

Both horizontal and vertical advection use a time step twice that of the adjustment stage thus $\Delta t_{adv} = 2\Delta t_{adj}$.

3.3.1 Vertical Advection

The Euler-backward time scheme is used. All quantities except q employ a centered difference in space.

First consider the temperature. The preliminary forward guess at level L is given by

$$T^*_L = T^n_L - \frac{0.5\Delta t_{adv}}{\Delta\eta_L}\left[\left(T^n_{L+1} - T^n_L\right)\dot{\eta}_{L+\frac{1}{2}} + \left(T^n_L - T^n_{L-1}\right)\dot{\eta}_{L-\frac{1}{2}}\right] \tag{27}$$

Recall that $\dot{\eta}$ is evaluated on layer interfaces thus $\dot{\eta}_{L+\frac{1}{2}}$ refers to the value on the interface between layers (or midlevels) L and L+1. The final backward step is

$$T^{n+1}_L = T^n_L - \frac{0.5\Delta t_{adv}}{\Delta\eta_L}\left[\left(T^*_{L+1} - T^*_L\right)\dot{\eta}_{L+\frac{1}{2}} + \left(T^*_L - T^*_{L-1}\right)\dot{\eta}_{L-\frac{1}{2}}\right] \tag{28}$$

The turbulent kinetic energy (Q2) is another prognostic variable that is advected (see Section 4.1 for a description of Q2). It is defined at height points on the layer interfaces and is zero at the upper boundary and at the ground. The vertical advection of Q2 is given by

$$Q2^*_{L+\frac{1}{2}} = Q2^n_{L+\frac{1}{2}} - 0.25\Delta t_{adv}\left[\left(Q2^n_{L+\frac{3}{2}} - Q2^n_{L+\frac{1}{2}}\right)\left(\dot{\eta}_{L+\frac{3}{2}} + \dot{\eta}_{L+\frac{1}{2}}\right)/\Delta\eta_{L+1}\right.$$
$$\left. + \left(Q2^n_{L+\frac{1}{2}} - Q2^n_{L-\frac{1}{2}}\right)\left(\dot{\eta}_{L+\frac{1}{2}} + \dot{\eta}_{L-\frac{1}{2}}\right)/\Delta\eta_L\right] \tag{29a}$$

$$Q2^{n+1}_{L+\frac{1}{2}} = Q2^n_{L+\frac{1}{2}} - 0.25\Delta t_{adv}\left[\left(Q2^*_{L+\frac{3}{2}} - Q2^*_{L+\frac{1}{2}}\right)\left(\dot{\eta}_{L+\frac{3}{2}} + \dot{\eta}_{L+\frac{1}{2}}\right)/\Delta\eta_{L+1}\right.$$
$$\left. + \left(Q2^*_{L+\frac{1}{2}} - Q2^*_{L-\frac{1}{2}}\right)\left(\dot{\eta}_{L+\frac{1}{2}} + \dot{\eta}_{L-\frac{1}{2}}\right)/\Delta\eta_L\right] \tag{29b}$$

The vertical advection of the velocity components is identical to that of the previous scalar quantities except that masses and vertical velocities, both defined at height points, must be averaged over velocity points. The quantity PDSL is the estimate of the pressure at $\eta = 1$ (mean sea level) at each height point and is obtained by dividing PD by η_s and adding p_T. The initial forward guess for the u and v components at level L is thus

$$u^*_L = u^n_L - \frac{0.5\Delta t_{adv}}{\overline{PDSL}^x}\left[\left(u^n_{L+1} - u^n_L\right)\overline{\left(\dot{\eta}_{L+\frac{1}{2}}PDSL\right)}^x + \left(u^n_L - u^n_{L-1}\right)\overline{\left(\dot{\eta}_{L-\frac{1}{2}}PDSL\right)}^x\right] \tag{30a}$$

$$v^*_L = v^n_L - \frac{0.5\Delta t_{adv}}{\overline{PDSL}^y}\left[\left(v^n_{L+1} - v^n_L\right)\overline{\left(\dot{\eta}_{L+\frac{1}{2}}PDSL\right)}^y + \left(v^n_L - v^n_{L-1}\right)\overline{\left(\dot{\eta}_{L-\frac{1}{2}}PDSL\right)}^y\right] \tag{30b}$$

and the backward step gives

$$u_L^{n+1} = u_L^n - \frac{0.5\Delta t_{adv}}{PDSL^x}\left[\left(u^*_{L+1}-u^*_L\right)\left(\dot\eta_{L+\frac12}PDSL\right)^x + \left(u^*_L-u^*_{L-1}\right)\left(\dot\eta_{L-\frac12}PDSL\right)^x\right] \quad (31a)$$

$$v_L^{n+1} = v_L^n - \frac{0.5\Delta t_{adv}}{PDSL^y}\left[\left(v^*_{L+1}-v^*_L\right)\left(\dot\eta_{L+\frac12}PDSL\right)^y + \left(v^*_L-v^*_{L-1}\right)\left(\dot\eta_{L-\frac12}PDSL\right)^y\right] \quad (31b)$$

The vertical advection of specific humidity is handled in a slightly different manner since it was determined that the vertical transport of moisture is described somewhat more accurately with an upstream spatial differencing. The forward guess is

$$q^*_L = q^n_L - \frac{.5\Delta t_{adv}}{\Delta\eta_L}\left\{\left(1-i_{L+1/2}\right)\left(q^n_{L+1}-q^n_L\right)\dot\eta_{L+1/2} + \left(1+i_{L-1/2}\right)\left(q^n_L-q^n_{L-1}\right)\dot\eta_{L-1/2}\right\} \quad (32)$$

where $i=\dot\eta/|\dot\eta|$.

A check is now made to preclude the appearance of negative moisture. Define TQA and TQB as follows:

$$TQA_L = .5\Delta t_{adv}\left(1-i_{L+1/2}\right)\left(q^*_{L+1}-q^*_L\right)\dot\eta_{L+1/2} \quad (33a)$$

$$TQB_L = .5\Delta t_{adv}\left(1+i_{L-1/2}\right)\left(q^*_L-q^*_{L-1}\right)\dot\eta_{L-1/2} - \xi_{L-1} \quad (33b)$$

$$TQB_1 = 0$$

The standard backward step yielding q_L^{n+1} is

$$q_L^{n+1} = q_L^n - \left(TQA_L + TQB_L\right)/\Delta\eta_L \quad (34)$$

To insure that q_L^{n+1} is always greater than $\epsilon\,(=10^{-12})$, the quantity TQA′ is introduced:

$$TQA'_L = TQA_L, \qquad q_L^{n+1} \geq \epsilon \quad (35a)$$

$$TQA'_L = \left(\epsilon - q_L^n\right)/\Delta\eta_L - TQB_L, \qquad q_L^{n+1} < \epsilon \quad (35b)$$

The amount of moisture created at this point is carried by $\xi = TQA' - TQA$. In order to conserve q, ξ must eventually be subtracted from the domain and is simply taken from the layer below as seen in (33b). Thus, the actual final backward step in the vertical advection of q is,

$$q_L^{n+1} = q_L^n - \left(TQA'_L + TQB_L\right)/\Delta\eta_L \quad (36)$$

3.3.2 Horizontal Advection

Janjic's (1984) horizontal advection scheme is used in conjunction with a modified Euler-backward time scheme. The modification is that the trial forward step is for $\sqrt{2}/2$ of an advective time step when considering non-momentum quantities. The result of this forward step is then used as the middle value in a centered difference to obtain the value at n+1. In

calculating the velocity components, the forward step is for precisely half an advective time step. This variation results in significantly less damping than occurs in the normal Euler-backward scheme for non-momentum quantities and no damping for momentum components.

For temperature the forward step at level L is

$$T_L^* = T_L^n - \frac{\Delta t_{adv}}{\sqrt{2}\,\Delta x\,\Delta y\,\Delta p_L}\{\frac{1}{3}[\overline{\{u_L\Delta y(\Delta p_L)^x\delta_x T_L^n\}}^x + \overline{\{v_L\Delta x(\Delta p_L)^y\delta_y T_L^n\}}^y]$$
$$+\frac{2}{3}[\overline{\{(u_L\Delta y + v_L\Delta x)^{y'}(\Delta p_L)^{x'}\delta_x T_L^n\}}^{x'}$$
$$+\overline{\{(-u_L\Delta y + v_L\Delta x)^{x'}(\Delta p_L)^{y'}\delta_y T_L^n\}}^{y'}]\} \qquad (37)$$

Using T^*_L as the temperature at the midpoint of the full advection time step, the new value at n+1 is

$$T_L^{n+1} = T_L^n - \frac{\Delta t_{adv}}{\Delta x\,\Delta y\,\Delta p_L}\{\frac{1}{3}[\overline{\{u_L\Delta y(\Delta p_L)^x\delta_x T^*_L\}}^x + \overline{\{v_L\Delta x(\Delta p_L)^y\delta_y T^*_L\}}^y]$$
$$+\frac{2}{3}[\overline{\{(u_L\Delta y + v_L\Delta x)^{y'}(\Delta p_L)^{x'}\delta_x T^*_L\}}^{x'}$$
$$+\overline{\{(-u_L\Delta y + v_L\Delta x)^{x'}(\Delta p_L)^{y'}\delta_y T^*_L\}}^{y'}]\} \qquad (38)$$

Specific humidity is handled precisely the same as the temperature.

Since turbulent energy is defined on layer interfaces while the velocity is at midlayers, an additional vertical averaging is necessary for horizontal advection of Q2. Let ADQ2A and ADQ2B represent the advection of Q2 by the velocity fields immediately above and below, respectively, with Q2A and Q2B being the resulting turbulent energies after the forward guess.

$$ADQ2A^*_{L+\frac{1}{2}} = -\frac{\Delta t_{adv}}{\sqrt{2}\,\Delta x\,\Delta y\,\Delta p_L}\{\frac{1}{3}[\overline{\{u_L\Delta y(\Delta p_L)^x\delta_x Q2^n_{L+\frac{1}{2}}\}}^x + \overline{\{v_L\Delta x(\Delta p_L)^y\delta_y Q2^n_{L+\frac{1}{2}}\}}^y]$$
$$+\frac{2}{3}[\overline{\{(u_L\Delta y + v_L\Delta x)^{y'}(\Delta p_L)^{x'}\delta_x Q2^n_{L+\frac{1}{2}}\}}^{x'}$$
$$+\overline{\{(-u_L\Delta y + v_L\Delta x)^{x'}(\Delta p_L)^{y'}\delta_y Q2^n_{L+\frac{1}{2}}\}}^{y'}]\} \qquad (39a)$$

$$ADQ2B^{*}_{L+\frac{1}{2}} = -\frac{\Delta t_{adv}}{\sqrt{2}\,\Delta x\,\Delta y\,\Delta p_L}\{\frac{1}{3}\left[\left(u_{L+1}\Delta y\left(\Delta p_{L+1}\right)^{x}\delta_x Q2^{n}_{L+\frac{1}{2}}\right)^{x} + \left(v_{L+1}\Delta x\left(\Delta p_{L+1}\right)^{y}\delta_y Q2^{n}_{L+\frac{1}{2}}\right)^{y}\right]$$

$$+\frac{2}{3}[\overline{\left\{\left(u_{L+1}\Delta y + v_{L+1}\Delta x\right)^{y'}\left(\Delta p_{L+1}\right)^{x'}\delta_x \cdot Q2^{n}_{L+\frac{1}{2}}\right\}^{x'}}$$

$$+\overline{\left\{\left(-u_{L+1}\Delta y + v_{L+1}\Delta x\right)^{x'}\left(\Delta p_{L+1}\right)^{y'}\delta_y \cdot Q2^{n}_{L+\frac{1}{2}}\right\}^{y'}}\,]\} \qquad (39b)$$

$$Q2A^{*}_{L+\frac{1}{2}} = Q2^{n}_{L+\frac{1}{2}} + ADQ2A^{*}_{L+\frac{1}{2}} \qquad (40a)$$

$$Q2B^{*}_{L+\frac{1}{2}} = Q2^{n}_{L+\frac{1}{2}} + ADQ2B^{*}_{L+\frac{1}{2}} \qquad (40b)$$

The centered step yields

$$ADQ2A^{n+1}_{L+\frac{1}{2}} = -\frac{\Delta t_{adv}}{\Delta x\,\Delta y\,\Delta p_L}\{\frac{1}{3}\left[\left(u_L\Delta y\left(\Delta p_L\right)^{x}\delta_x Q2A^{*}_{L+\frac{1}{2}}\right)^{x} + \left(v_L\Delta x\left(\Delta p_L\right)^{y}\delta_y Q2A^{*}_{L+\frac{1}{2}}\right)^{y}\right]$$

$$+\frac{2}{3}[\overline{\left\{\left(u_L\Delta y + v_L\Delta x\right)^{y'}\left(\Delta p_L\right)^{x'}\delta_x \cdot Q2A^{*}_{L+\frac{1}{2}}\right\}^{x'}}$$

$$+\overline{\left\{\left(-u_L\Delta y + v_L\Delta x\right)^{x'}\left(\Delta p_L\right)^{y'}\delta_y \cdot Q2A^{*}_{L+\frac{1}{2}}\right\}^{y'}}\,]\} \qquad (41a)$$

$$ADQ2B^{n+1}_{L+\frac{1}{2}} = -\frac{\Delta t_{adv}}{\Delta x\,\Delta y\,\Delta p_L}\{\frac{1}{3}\left[\left(u_{L+1}\Delta y\left(\Delta p_{L+1}\right)^{x}\delta_x Q2A^{*}_{L+\frac{1}{2}}\right)^{x} + \left(v_{L+1}\Delta x\left(\Delta p_{L+1}\right)^{y}\delta_y Q2A^{*}_{L+\frac{1}{2}}\right)^{y}\right]$$

$$+\frac{2}{3}[\overline{\left\{\left(u_{L+1}\Delta y + v_{L+1}\Delta x\right)^{y'}\left(\Delta p_{L+1}\right)^{x'}\delta_x \cdot Q2A^{*}_{L+\frac{1}{2}}\right\}^{x'}}$$

$$+\overline{\left\{\left(-u_{L+1}\Delta y + v_{L+1}\Delta x\right)^{x'}\left(\Delta p_{L+1}\right)^{y'}\delta_y \cdot Q2A^{*}_{L+\frac{1}{2}}\right\}^{y'}}\,]\} \qquad (41b)$$

$$Q2^{n+1}_{L+\frac{1}{2}} = Q2^{n}_{L+\frac{1}{2}} + 0.5\left(ADQ2A^{n+1}_{L+\frac{1}{2}} + ADQ2B^{n+1}_{L+\frac{1}{2}}\right) \qquad (42)$$

The horizontal advection of the wind components is nearly identical to that for T and q except that mass fluxes must be averaged over height points and the layer masses must be averaged over velocity points. Define the following auxiliary quantities:

$$UEW = \left(\delta_x u_L\right)\left(\left(u_L \Delta y\right)\overline{\Delta p_L}^{x}\right)^{x} \qquad UNS = \left(\delta_y \bar{u}_L\right)\left(\left(\Delta x v_L\right)\overline{\Delta p_L}^{y}\right)^{x} \tag{43}$$

$$UNE = \left(\delta_{x'} u_L\right)\left(\left(\overline{u_L \Delta y + v_L \Delta x}^{y'}\right)\left(\overline{\Delta p_L}^{x'}\right)^{x}\right)$$

$$USE = \left(\delta_{y'} u_L\right)\left(\left(\overline{-u_L \Delta y + v_L \Delta x}^{x'}\right)\left(\overline{\Delta p_L}^{y'}\right)^{x}\right)$$

$$VEW = \left(\delta_x v_L\right)\left(\left(u_L \Delta y\right)\overline{\Delta p_L}^{x}\right)^{y} \qquad VNS = \left(\delta_y v_L\right)\left(\left(v_L \Delta x\right)\overline{\Delta p_L}^{y}\right)^{y} \tag{44}$$

$$VNE = \left(\delta_{x'} v_L\right)\left(\left(\overline{u_L \Delta y + v_L \Delta x}^{y'}\right)\left(\overline{\Delta p_L}^{x'}\right)^{y}\right)$$

$$VSE = \left(\delta_{y'} v_L\right)\left(\left(\overline{u_L \Delta y + v_L \Delta x}^{x'}\right)\left(\overline{\Delta p_L}^{y'}\right)^{y}\right)$$

Note that UEW, UNS, VEW, and VNS are defined at the center of each grid box, UNE and VNE are defined on the northwest side and USE and VSE are defined on the southwest side of each box.

The trial forward step at level L is then

$$u^* = u^n - \frac{\Delta t_{adv}}{2\Delta x \Delta y \overline{\Delta p}^{x}}\left[\frac{1}{3}\left(\overline{UEW}^{x} + \overline{UNS}^{y}\right) + \frac{2}{3}\left(\overline{UNE}^{x'} + \overline{USE}^{y'}\right)\right] \tag{45a}$$

$$v^* = v^n - \frac{\Delta t_{adv}}{2\Delta x \Delta y \overline{\Delta p}^{y}}\left[\frac{1}{3}\left(\overline{VEW}^{x} + \overline{VNS}^{y}\right) + \frac{2}{3}\left(\overline{VNE}^{x'} + \overline{VSE}^{y'}\right)\right] \tag{45b}$$

and the final centered step is

$$u^{n+1} = u^n - \frac{\Delta t_{adv}}{\Delta x \Delta y \overline{\Delta p}^{x}}\left[\frac{1}{3}\left(\overline{UEW^*}^{x} + \overline{UNS^*}^{y}\right) + \frac{2}{3}\left(\overline{UNE^*}^{x'} + \overline{USE^*}^{y'}\right)\right] \tag{46a}$$

$$v^{n+1} = v^n - \frac{\Delta t_{adv}}{\Delta x \Delta y \overline{\Delta p}^{y}}\left[\frac{1}{3}\left(\overline{VEW^*}^{x} + \overline{VNS^*}^{y}\right) + \frac{2}{3}\left(\overline{VNE^*}^{x'} + \overline{VSE^*}^{y'}\right)\right] \tag{46b}$$

where the starred quantities use the velocity components derived from (45a) and (45b). Through algebraic manipulation of (46) with the continuity equation, it can be shown that both momentum and kinetic energy are conserved by this scheme.

3.3.3 Upstream Advection Near Boundaries

Because insufficient information is available for the advection scheme within the five outer rows of the domain's horizontal boundaries, an upstream scheme is used for points in the third, fourth, and fifth outermost rows (no prediction occurs in the outer two rows; see Section 5).

In the case of temperature, mean velocity components are found at the height point in question by four-point averaging the surrounding velocities and thereby defining the means as

$$\bar{u}^{xy} = 0.5\left(\bar{u}^{x} + \bar{u}^{y}\right) \tag{47a}$$

$$\bar{v}^{xy} = 0.5\left(\bar{v}^{x} + \bar{v}^{y}\right) \tag{47b}$$

The assumption is now made that the wind upstream of this height point is the same as at the point itself thus the direction of the mean wind is reversed and it is multiplied by half an advective time step to determine the location from which advection needed to obtain the half time step values is originating. Bilinear interpolation to this location from the four surrounding points will yield the temperature at the height point after the half time step advection has occurred. Using the updated wind and temperature values, the procedure is repeated using the full advection time step. As was done in the previous section, the first step is forward by $(\sqrt{2}/2)\Delta t_{adv}$ for the non-momentum quantities.

To see this procedure quantitatively, consider Fig. 6 which depicts the central height point where T_0 is being predicted. The X shows the point from which the upstream advection is originating. PP and QP are the distances from T_0 to X along the x′ and y′ axes, respectively, with the grid interval d chosen as the unit distance. T_1, T_2 and T_3 are the three temperatures which complete the square surrounding X. The values of PP and QP are given by

$$PP = -\frac{\Delta t_{adv}}{4\Delta x \Delta y}\left[\bar{u}^{xy}\Delta y + \bar{v}^{xy}\Delta x\right] \tag{48a}$$

$$QP = -\frac{\Delta t_{adv}}{4\Delta x \Delta y}\left[-\bar{u}^{xy}\Delta y + \bar{v}^{xy}\Delta x\right] \tag{48b}$$

Note that the 4 multiplying Δx and Δy represents the product of the divisor, 2, of Δt and two $\sqrt{2}$ factors. The first $\sqrt{2}$ accounts for the unit length along the primed axes and the second converts u and v to u′ and v′ as seen in Fig. 5. Define the following bilinear interpolating coefficients:

```
F0=1-PP-QP-(PP)(QP)
F1=PP(1-QP)                    (49)
F2=QP(1-PP)
F3=(PP)(QP)
```

For simplicity, the quantity FF=F0-1 will be used in the following equations to avoid writing the explicit subtraction of each quantity at the zero location in Fig. 6. The initial forward guess in the time scheme is then written as

Since the topography can extend to within two rows of the edge of the domain, some of the points needed for the computation may be underground.

$$T^*_0 = T^n_0 + \sqrt{2}[FF\ T^n_0 + F1\ T^n_1 + F2\ T^n_2 + F3\ T^n_3] \tag{50}$$

The initial forward step is done for T, q, and Q2 as well as the velocity components which will be described below. With the new wind component estimates, (48) and (49) are recalculated. Then the updated temperature at level L near the boundaries is

$$T^{n+1}_0 = T^n_0 + 2[FF*T^*_0 + F1*T^*_1 + F2*T^*_2 + F3*T^*_3] \tag{51}$$

where the F^*'s indicate the recalculated values.

~~Due to the presence of topography, lateral boundaries in eta layers will occur at the sides of steps as well as at the edge of the domain.~~ If T_1, T_2, or T_3 in Fig. 6 is submerged, realistic values must be used in their place for the upstream algorithm to be used. Table 1 lists the various contingencies for submerged points.

The upstream advection of specific humidity is handled in precisely the same manner as the temperature, ~~except that values of submerged points are zero.~~ The same averaging rationale previously described for the advection of turbulent energy is also used for upstream advection. Let ADQ2A and ADQ2B represent the advection of Q2 by the velocity field immediately above and below level $L+\frac{1}{2}$ on which Q2 resides and again let Q2A and Q2B represent the resulting turbulent energy. Whereas all the F's in (49) were evaluated at level L, those associated with Q2B must now use values at level L+1. The resulting forward guess is

$$ADQ2A^*_{L+\frac{1}{2}} = FF_L Q2^n_0 + F1_L Q2^n_1 + F2_L Q2^n_2 + F3_L Q2^n_3 \tag{52a}$$

$$ADQ2B^*_{L+\frac{1}{2}} = FF_{L+1} Q2^n_0 + F1_{L+1} Q2^n_1 + F2_{L+1} Q2^n_2 + F3_{L+1} Q2^n_3 \tag{52b}$$

$$Q2A^*_{L+\frac{1}{2}} = Q2^n_0 + \sqrt{2}\,ADQ2A^*_{L+\frac{1}{2}} \tag{53a}$$

$$Q2B^*_{L+\frac{1}{2}} = Q2^n_0 + \sqrt{2}\,ADQ2B^*_{L+\frac{1}{2}} \tag{53b}$$

where the subscripts on Q2 indicate the same locations on level $L+\frac{1}{2}$ as for T in Fig. 6.

Let ADQ2A** and ADQ2B** represent the new values of advection calculated in (52) using Q2A* and Q2B* in place of Q2 and with new F's taken from the forward guess wind components. Then the final update of Q2 yields

$$Q2^{n+1}_0 = Q2^n_0 + ADQ2A^{**}_{L+\frac{1}{2}} + ADQ2B^{**}_{L+\frac{1}{2}} \tag{54}$$

The upstream advection of velocity is treated in the same manner except that no averaging is necessary to determine the advecting wind, i.e., each component is advected by the total wind at its location. The initial forward step at level L is thus

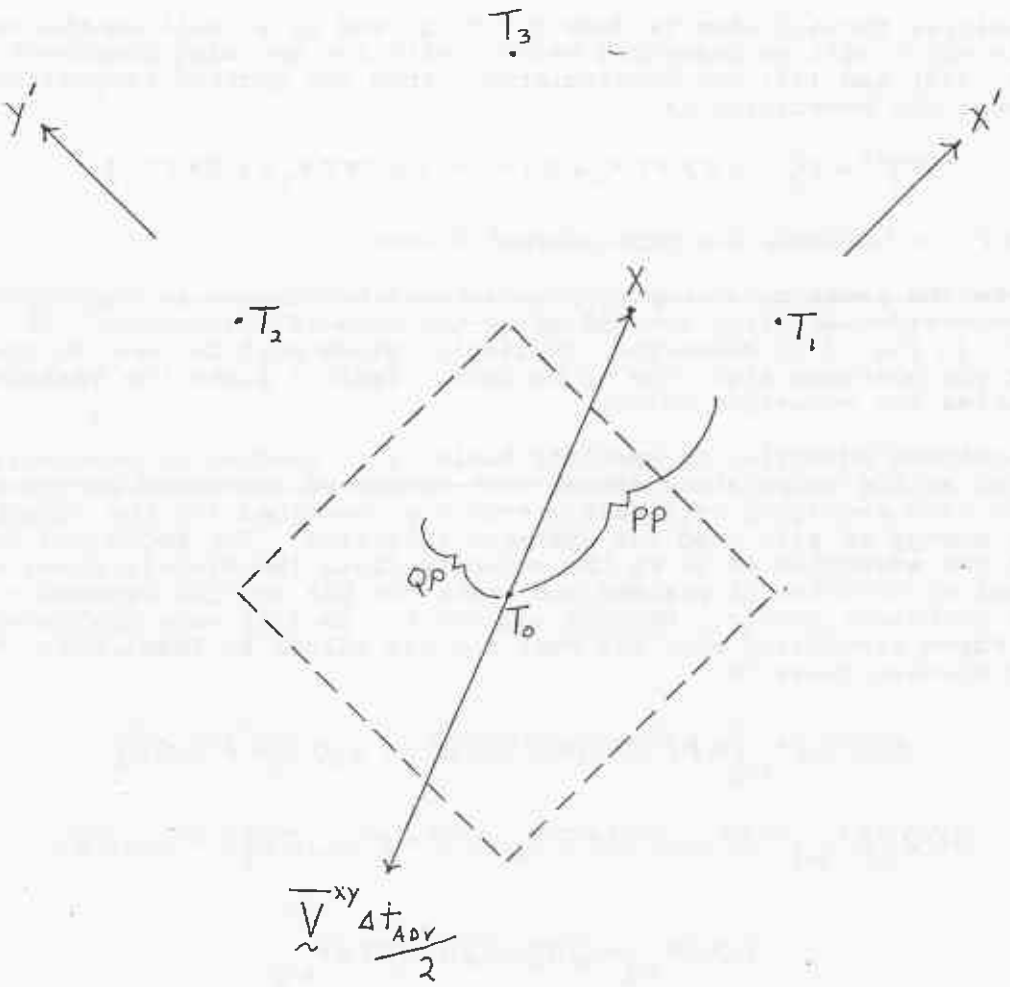

Fig. 6. Upstream advection of temperature from point X by wind $\underset{\sim}{\overline{V}}^{xy}$.

$$u^*_0 = u^n_0 + FFu^n_0 + F1u^n_1 + F2u^n_2 + F3u^n_3 \qquad (55a)$$

$$v^*_0 = v^n_0 + FFv^n_0 + F1v^n_1 + F2v^n_2 + F3v^n_3 \qquad (55b)$$

and the final centered step is

$$u^{n+1}_0 = u^n_0 + 2\left(FF^*u^*_0 + F1^*u^*_1 + F2^*u^*_2 + F3^*u^*_3\right) \qquad (56a)$$

$$v^{n+1}_0 = v^n_0 + 2\left(FF^*v^*_0 + F1^*v^*_1 + F2^*v^*_2 + F3^*v^*_3\right) \qquad (56b)$$

As with ~~specific humidity and~~ turbulent energy, submerged velocity components needed with upstream advection are equal to zero.

3.4 Smoothing Specific Humidity

Negative specific humidities can occur in regions where q is very small and/or where large gradients of q occur. If after the advection any η layer contains $q < -2 \times 10^{-12} kgkg^{-1}$, smoothing is carried out on that layer such that

$$q^{n+1}_{new} = q^{n+1}_{old} + .125\ \{\delta^2_x\left(q^{n+1}_{old}\right) + \delta^2_y\left(q^{n+1}_{old}\right)\} \qquad (57)$$

Smoothing is used rather than setting to zero to avoid anomalous sources of moisture.

3.5 Horizontal Diffusion

After each adjustment time step a nonlinear fourth order diffusion is applied to the temperature, specific humidity, and wind components in each eta layer. The magnitude of the diffusion is proportional to the deformation and the turbulent energy. Let DEFT and DEFS be defined at height points and denote the stretching and shearing deformation, respectively:

$$DEFT = \delta_x u - \delta_y v \qquad (58a)$$

$$DEFS = \delta_y u + \delta_x v \qquad (58b)$$

The total deformation at level L is modified by the turbulent energy to yield

$$DEF = \left(DEFT^2 + DEFS^2 + 50\ Q2_{L+1}\right)^{\frac{1}{2}} \qquad (59)$$

→ 50Q2

where $16 \le DEF \le 32$.

The second order diffusive correction for temperature defined at height points is given by

Table 1. Values used for underground temperatures with upstream advection. Subscripts refer to locations in Fig. 6.

Submerged Points	Substituted Value
T_1	$T_1 = T_0 + T_3 - T_2$
T_2	$T_2 = T_0 + T_3 - T_1$
T_3	$T_3 = T_1 + T_2 - T_0$
T_1, T_3	$T_1 = T_0 \quad T_3 = T_2$
T_2, T_3	$T_2 = T_0 \quad T_3 = T_1$

$$TDIF = \frac{c_0 c_1 ACDT}{\Delta x' \Delta y'} \left\{ \delta_x \cdot \left(\overline{DEF}^{x'} \delta_x \cdot T \right) + \delta_y \cdot \left(\overline{DEF}^{y'} \delta_y \cdot T \right) \right\} \qquad (60)$$

where $ACDT$ was defined in conjunction with Eq. (20) and $c_0 = 1.25$. The diffusion is increased around the lateral boundaries by setting $c_1 = 8$ in the ~~five~~ outer ~~rows~~ while it equals 1 on the remainder of the grid. The modified temperature then becomes $T^{(3)} = T + TDIF$, where the superscript denotes the result after second order smoothing. The process is now repeated to produce a new T with fourth order diffusion:

$$T^{(4)} = T^{(2)} - \frac{c_0 c_1 ACDT}{\Delta x' \Delta y'} \left\{ \delta_x \cdot \left(\overline{DEF}^{x'} \delta_x \cdot TDIF \right) + \delta_y \cdot \left(\overline{DEF}^{y'} \delta_y \cdot TDIF \right) \right\} \qquad (61)$$

The diffusion of specific humidity is identical to that of temperature.

In order to calculate the diffusion of momentum, consider the quantities UDIF and VDIF defined at velocity points:

$$UDIF = \frac{c_1 ACDT}{\Delta x' \Delta y'} \left\{ \delta_x \cdot \left(\overline{DEF}^{y'} \delta_x \cdot u \right) + \delta_y \cdot \left(\overline{DEF}^{x'} \delta_y \cdot u \right) \right\} \qquad (62a)$$

$$VDIF = \frac{c_1 ACDT}{\Delta x' \Delta y'} \left\{ \delta_x \cdot \left(\overline{DEF}^{y'} \delta_x \cdot v \right) + \delta_y \cdot \left(\overline{DEF}^{x'} \delta_y \cdot v \right) \right\} \qquad (62b)$$

The second order modifications are analogous to those for T. The final values for u and v are then

$$u^{(4)} = u^{(2)} - \frac{c_1 ACDT}{\Delta x' \Delta y'} \left\{ \delta_x \cdot \left(\overline{DEF}^{y'} \delta_x \cdot UDIF \right) + \delta_y \cdot \left(\overline{DEF}^{x'} \delta_y \cdot UDIF \right) \right\} \qquad (63a)$$

$$v^{(4)} = v^{(2)} - \frac{c_1 ACDT}{\Delta x' \Delta y'} \left\{ \delta_x \cdot \left(\overline{DEF}^{y'} \delta_x \cdot VDIF \right) + \delta_y \cdot \left(\overline{DEF}^{x'} \delta_y \cdot VDIF \right) \right\} \qquad (63b)$$

If either term in any of the above differences involves an underground wind component then the difference itself is set to zero. It may be shown that the strength of this fourth order diffusion is proportional to the time derivative of the second order diffusion.

4 Physical Parameterizations

The eta model's physical package describes turbulent exchange, large scale and convective precipitation, surface processes, and radiation. Turbulence and convection are called every four adjustment time steps while large scale precipitation is called every two. Radiation is called every 30 adjustment time steps. The quantity Δt_{phy} will equal 4 Δt_{adj}.

4.1 Turbulent Exchange

The process of turbulent transfer is described in the eta model by applying Mellor-Yamada second order closure theory (Mellor and Yamada, 1974, 1982) which yields exchange coefficients used to calculate the heat, moisture, and momentum exchange through model layer interfaces. Different "levels" of the theory are used in the lowest layer above the ground and in the free atmosphere in all higher layers.

4.1.1 Exchange in the Free Atmosphere: Level 2.5

The so-called Level 2.5 of the heirarchy developed by Mellor and Yamada involves not only the model variables which will undergo the transfer but also a quantity called turbulent energy (Q2) defined as twice the turbulent kinetic energy per unit mass. Predicting this quantity is the fundamental problem in finding the exchange coefficients. The prognostic equation for Q2 is

$$\frac{\partial Q2}{\partial t} = -\vec{V}\cdot\nabla_\eta Q2 - \dot{\eta}\frac{\partial Q2}{\partial \eta} + \frac{\partial}{\partial z}\left(l\ Q\ S_q\ \frac{\partial Q2}{\partial z} \right) + 2\left(P_s + P_b - \epsilon\right) \quad . \quad (64)$$

The first two terms on the right hand side of (64) are the advection, the third term is the diffusion, and the last terms are the production / dissipation. Each of these three processes is calculated separately in a split fashion. The advection of Q2 was already described in Section 3.3.

Recall that Q2 is defined at the layer interfaces since exchange takes place there. Initially Q2 is assigned a value of $10^{-4} m^2/s^2$ everywhere except at the top of the domain, at the earth's surface, and on the outermost row where it is set to zero throughout the forecast.

To find the production/dissipation of Q2, a variety of other quantities must first be calculated. The principal length scale l is found from

$$l_{L+\frac{1}{2}} = \frac{l_0\ k\ z_{L+\frac{1}{2}}}{k\ z_{L+\frac{1}{2}} + l_0} \quad (65a)$$

the quantity Q in the diffusion term is equal to $(Q2)^{1/2}$.

$$l_0 = \frac{\alpha \sum_{L=LM}^{1} (\bar{z}^{\eta}_{L} \bar{Q}^{\eta}_{L}) \Delta p_L}{\sum_{L=LM}^{1} (\bar{Q}^{\eta}_{L}) \Delta p_L} \quad , \; l_0 \leq 90 \; m \tag{65b}$$

where:

k is the von Karman constant (0.4),

$\alpha = 0.1$, z is the altitude above the ground,

Δp_L is the pressure depth of η layer L,

LM is the lowest midlayer level above the ground, and $Q = (Q2)^{\frac{1}{2}}$

The bars over z and Q indicate vertical means for layer L since these variables are defined only at the top and bottom of each layer.

All subsequent auxiliary quantities regarding Q2 will be defined at height points on layer interfaces. Define GH and GM such that

$$GH_{L+\frac{1}{2}} = -\left(\frac{l_{L+\frac{1}{2}}}{Q_{L+\frac{1}{2}}} \right)^2 \beta g \frac{\partial \theta_v}{\partial z} \tag{66a}$$

$$GM_{L+\frac{1}{2}} = \left(\frac{l_{L+\frac{1}{2}}}{Q_{L+\frac{1}{2}}} \right)^2 \left[\left(\frac{\partial u}{\partial z} \right)^2 + \left(\frac{\partial v}{\partial z} \right)^2 \right] \tag{66b}$$

where:

$\beta = 3.67 \times 10^{-3}$, g is 9.8 and θ_v is the virtual potential temperature.

GH is not allowed to exceed 0.032 while GM may not exceed 0.48 GH. Bearing in mind that u, v, and θ_v are carried at midlayers, their derivatives in (66a) and (66b) are

$$\frac{\partial (u,v)}{\partial z} \cong \frac{\overline{(u,v)}^{xy}_{L} - \overline{(u,v)}^{xy}_{L+1}}{z_{L-\frac{1}{2}} - z_{L+\frac{3}{2}}} \tag{62a}$$

$$\frac{\partial \theta_v}{\partial z} \cong \frac{\theta_{vL} - \theta_{vL+1}}{z_{L-\frac{1}{2}} - z_{L+\frac{3}{2}}} \tag{62b}$$

Before (67b) is used, the θ_v field is smoothed according to:

$$\theta_v(new) = \theta_v(old) + 0.125 \left\{ \delta^2_x \left(\theta_v(old) \right) + \delta^2_y \left(\theta_v(old) \right) \right\} \tag{68}$$

Now the quantities SH and SM must be found by simultaneous solution of the following relations:

$$SM\left[6A_1A_2\ GM\right]+SH\left[1-3A_2B_2\ GH-12A_1A_2\ GH\right]=A_2 \qquad (69)$$

$$SM\left[1+6A_1^2\ GM-9A_1A_2\ GH\right]-SH\left[12A_1^2\ GH+9A_1A_2\ GH\right]=A_1\left(1-3C_1\right)$$

where
$A_1=.92$, $B_1=16.6$, $A_2=0.74$, $B_2=10.1$, $C_1=0.08$.

Through manipulation of equations described by Mellor and Yamada, the production / dissipation term can be written

$$P_s+P_b-\epsilon=\frac{Q^3}{l}\left\{SM\ GM+SH\ GH\ -B_1^{-1}\right\} \qquad (70)$$

Expressing the left hand side of (70) as the finite difference time change of Q2, using the fact that $\partial(Q2/2)/\partial t=Q\partial Q/\partial t$, and using Q at time n+1 on the right hand side of (70), then it follows that

$$\frac{X\ \Delta t_{phy}}{l}\left(Q^{n+1}\right)^2-Q^{n+1}+Q^n\ =\ 0 \qquad (71)$$

where X represents the bracketed terms in (70). Eq.(71) is a simple quadratic equation which is solved for Q^{n+1}:

$$Q^{n+1}=\frac{l}{2\ X\ \Delta t_{phy}}\left\{\ 1-\left(1-\frac{4X\Delta t_{phy}Q^n}{l}\right)^{\frac{1}{2}}\ \right\} \qquad (72)$$

The negative square root is taken in (72) since the positive root yields an un-physical computational solution. Eq.(72) is solved at each layer interface below the top of the domain and above the surface.

Now Q2 will be updated with the diffusion term in (64). The prognostic equation is cast into finite difference form as follows:

$$\frac{Q2^{n+1}_{L+\frac{1}{2}}-Q2^{n}_{L+\frac{1}{2}}}{\Delta t_{phy}}=\frac{S_q}{z_{L-\frac{1}{2}}-z_{L+\frac{3}{2}}}\left\{\left(l_{L-\frac{1}{2}}Q^n_{L-\frac{1}{2}}+l_{L+\frac{1}{2}}Q^n_{L+\frac{1}{2}}\right)\left(\frac{Q2^n_{L-\frac{1}{2}}-Q2^{n+1}_{L+\frac{1}{2}}}{z_{L-\frac{1}{2}}-z_{L+\frac{1}{2}}}\right)\right.$$

$$\left.-\left(l_{L+\frac{1}{2}}Q^n_{L+\frac{1}{2}}+l_{L+\frac{3}{2}}Q^n_{L+\frac{3}{2}}\right)\left(\frac{Q2^{n+1}_{L+\frac{1}{2}}-Q2^n_{L+\frac{3}{2}}}{z_{L+\frac{1}{2}}-z_{L+\frac{3}{2}}}\right)\ \right\} \qquad (73)$$

where $S_q=0.2$. Note that the pseudo-implicit form of (73) is analogous to that used in the Dufort-Frankel scheme. With some algebra, (73) is solved for $Q2^{n+1}$ to give

$$Q2^{n+1}_{L+\frac{1}{2}}=\left\{\frac{Q2^n_{L+\frac{1}{2}}+F1\ Q2^n_{L-\frac{1}{2}}+F2\ Q2^n_{L+\frac{3}{2}}}{1+F1+F2}\ \right\} \qquad (74)$$

where

$$F1 = F3\left(\frac{l_{L-\frac{1}{2}}Q^{n}_{L-\frac{1}{2}} + l_{L+\frac{1}{2}}Q^{n}_{L+\frac{1}{2}}}{z_{L-\frac{1}{2}} - z_{L+\frac{1}{2}}}\right) \tag{75a}$$

$$F2 = F3\left(\frac{l_{L+\frac{1}{2}}Q^{n}_{L+\frac{1}{2}} + l_{L+\frac{3}{2}}Q^{n}_{L+\frac{3}{2}}}{z_{L+\frac{1}{2}} - z_{L+\frac{3}{2}}}\right) \tag{75b}$$

$$F3 = \frac{\Delta t_{phy} S_q}{z_{L-\frac{1}{2}} - z_{L+\frac{3}{2}}} \tag{75c}$$

Q2 has now been fully updated according to (64) and is constrained to be no greater than $10^3 (m/s)^2$. Before proceeding, the field is smoothed:

$$Q2(new) = Q2(old) + .125\ \left\{\ \delta_x^2 (Q2(old)) + \delta_y^2 (Q2(old))\ \right\} \tag{76}$$

The final step is to evaluate the exchange coefficients and apply them to the mixing of model variables. The formulas for the heat and momentum exchange coefficients, respectively, are

$$KH_{L+\frac{1}{2}} = l_{L+\frac{1}{2}} Q_{L+\frac{1}{2}} SH_{L+\frac{1}{2}} \tag{77a}$$

$$KM_{L+\frac{1}{2}} = l_{L+\frac{1}{2}} Q_{L+\frac{1}{2}} SM_{L+\frac{1}{2}} \tag{77b}$$

The value of Q has changed since l, SH, and SM were first calculated so the latter are now re-evaluated using (65), (66), (67), and (69) before finding KH and KM which are not allowed to exceed $10^3 m^2/s$ or to be negative.

The turbulent exchange is then

$$\frac{\partial(\theta, q)}{\partial t} = \frac{1}{\rho}\frac{\partial}{\partial z}\left(\rho KH \frac{\partial(\theta, q)}{\partial z}\right) \tag{78a}$$

$$\frac{\partial(u, v)}{\partial t} = \frac{1}{\rho}\frac{\partial}{\partial z}\left(\rho KM \frac{\partial(u, v)}{\partial z}\right) \tag{78b}$$

where ρ is the air density. The same strategy is used to solve these equations as was used in (73) to handle the diffusion of Q2. As an example, consider the finite difference form of (78a) for potential temperature:

$$\frac{\theta_L^{n+1}-\theta_L^n}{\Delta t_{phy}} = \frac{1}{\rho_L\left(z_{L-\frac{1}{2}}-z_{L+\frac{1}{2}}\right)}\left\{\left(\rho_{L-1}+\rho_L\right)KH_{L-\frac{1}{2}}\left(\frac{\theta_{L-1}^n-\theta_L^{n+1}}{z_{L-\frac{3}{2}}-z_{L+\frac{1}{2}}}\right)\right.$$

$$\left.-\left(\rho_L+\rho_{L+1}\right)KH_{L+\frac{1}{2}}\left(\frac{\theta_L^{n+1}-\theta_{L+1}^n}{z_{L-\frac{1}{2}}-z_{L+\frac{3}{2}}}\right)\right\} \tag{79}$$

Solving for θ_L^{n+1} yields

$$\theta_L^{n+1} = \frac{\rho_L\theta_L^n + F1\ \theta_{L-1}^n + F2\ \theta_{L+1}^n}{\rho_L + F1\ + F2} \tag{80}$$

where

$$F1 = \frac{F3\ \left(\rho_{L-1}+\rho_L\right)KH_{L-\frac{1}{2}}}{z_{L-\frac{3}{2}}-z_{L+\frac{1}{2}}} \tag{81a}$$

$$F2 = \frac{F3\ \left(\rho_{L+1}+\rho_L\right)KH_{L+\frac{1}{2}}}{z_{L-\frac{1}{2}}-z_{L+\frac{3}{2}}} \tag{81b}$$

$$F3 = \frac{\Delta t_{phy}}{z_{L-\frac{1}{2}}-z_{L+\frac{1}{2}}} \tag{81c}$$

For specific humidity, q simply replaces θ in (79) and (80).

Calculating the mixing of the wind components is precisely analogous to that for θ and q except that KM replaces KH and since ρ (through the pressure, temperature, and specific humidity), z, and KM are calculated at height points, they must first be four-point averaged over velocity points. Underground values of ρ and T are set at 10^{-4} kg m^{-3} and 100°K, respectively.

4.1.2 Exchange at the Surface: Level 2

At the ground and sea surface, a simplifying assumption is made to Level 2.5, namely that the local derivative, advection, and diffusion of Q2 in (64) are zero. In other words, the production and dissipation of turbulent energy are balanced. The stability of the surface layer as reflected by the gradient Richardson number (R_i) is the primary factor which will determine mixing.

R_i is defined by

$$R_i = \frac{g\beta\Delta\theta_v\Delta z}{\Delta(u^2+v^2)} \tag{82}$$

Since the exchange will take place between the lowest midlayer predictive model level and the ground or ocean, the depth of this interval is needed as are surface boundary values for θ_v, u and v. At the lower boundary, the wind components are always zero thus the denominator of (82) is simply u^2+v^2 and must lie between .0001 and 2500 $(m/s)^2$. The virtual potential temperature is given by

$$\theta_v = \theta_{s/c}\left[1+0.61\ q_{sat}\ (WET/WFC)\right] \tag{83}$$

where q_{sat} is the saturation specific humidity given the temperature of and pressure at the surface. WET is the soil moisture and WFC is the maximum value of soil moisture (0.1125 m). Over the ocean, WET/WFC is always 1.

To find the depth of the model's lowest half-layer through which exchange will occur, one must account for the logarithmic profile that is assumed for a quantity f below the critical level of $z_c(=2m)$: $f=f+C\ln(z/z_0)$, where z_0 is the roughness length. From z_c up to the lowest midlayer eta level, the profiles are assumed to be linear: f=A+Bz. If both zero and first order continuity of these two profiles exists at z_c, then A, B, and C for each f can be found in terms of known quantities:

$$A = f_{LM} - Bz_{LM} \tag{84a}$$

$$C = Bz_c \tag{84b}$$

$$B = \frac{f_{LM}-f_{s/c}}{z_{LM}+z_c\left[\ln(z_c/z_0)-1\right]} \tag{84c}$$

where LM denotes the lowest midlayer point above the surface. The quantity Δz needed in (82) is seen to be the denominator in (84c). However, the roughness length is still unknown. Currently the model uses $z_0=0.1+10^{-5}\phi_{s/c}$ over land ($\phi_{s/c}$ is the surface geopotential) and Charnock's relation over water:

$$z_0 = \left(\frac{a}{g}\right)u_*^2 \text{ where a= } 0.016m^{-1} \text{ and } \quad u_* = \frac{k\,|\vec{V}_c|}{\ln\left(\frac{z_c}{z_0}\right)}.$$

Using the relations in (84) and the fact that $\vec{V}_c = A + Bz_c$, then

$$u_*^2 = \frac{k^2 z_c^2 \left|\vec{V}_c\right|^2}{\left[z_{LM} + z_c\left(\ln\left(z_c / z_0\right) - 1\right)\right]^2} \tag{85}$$

The value of z_0 used in (85) is that from the previous time step. The initial value of z_0, over the ocean is assumed to be $10^{-3}m$ and is never allowed to be less than $10^{-4}m$.

Once z_0 is updated (over ocean) then Δz can be found everywhere and R_i is evaluated from (82). Now define Γ as follows:

$$\Gamma = \frac{R_f}{1 - R_f} \tag{86a}$$

$$R_f = 0.664\left[R_i + 0.1765 - \left(R_i^2 - 0.3175 R_i + 0.0312\right)^{\frac{1}{2}}\right] \tag{86b}$$

where R_f is the flux Richardson number which is constrained to be no less than -0.38. The auxiliary stability functions SH and SM are given by

$$\tilde{S}H = 3A_2\left(\gamma_1 - \gamma_2 \Gamma\right) \tag{87a}$$

$$\tilde{S}M = \frac{3A_1\left(\gamma_1 - \gamma_2\Gamma\right)\left[\gamma_1 - C_1 - \left(6A_1 + 3A_2\right)\Gamma B_1^{-1}\right]}{\gamma_1 - \gamma_2\Gamma + 3A_1\Gamma B_1^{-1}} \tag{87b}$$

where

$$\gamma_1 = \frac{1}{3} - 2A_1 B_1^{-1} \tag{88a}$$

$$\gamma_2 = \left(B_2 + 6A_1\right)B_1^{-1} \tag{88b}$$

and A_1, B_1, A_2, B_2, and C_1 are the same as in Level 2.5.

If R_f ever exceeds 0.19, stability is too great for turbulent exchange to occur, so R_f is set back to 0.19 and SH and SM are set to zero. Finally the actual stability functions are

$$SH = \left(B_1\left(1 - R_f\right)\tilde{S}M\right)^{\frac{1}{2}}\tilde{S}H \tag{89a}$$

$$SM = \left(B_1\left(1 - R_f\right)\tilde{S}M\right)^{\frac{1}{2}}\tilde{S}M \tag{89b}$$

which lead to the surface exchange coefficients

$$KHS = \frac{l_{LM-\frac{1}{2}}SH}{4[illegible]}\left\{\left(\bar{u}_{LM}^{xy}\right)^2 + \left(\bar{v}_{LM}^{xy}\right)^2\right\}^{\frac{1}{2}} \tag{90a}$$

$$KMS = \frac{l_{LM-\frac{1}{2}}SM}{4[illegible]}\left\{\left(\bar{u}_{LM}^{xy}\right)^2 + \left(\bar{v}_{LM}^{xy}\right)^2\right\}^{\frac{1}{2}} \tag{90b}$$

The length scale at the top of the lowest layer, $l_{LM-\frac{1}{2}}$, is divided by four in (90) to approximate the length scale midway between the surface and level LM. Since (90b) gives the momentum coefficients over height points, KMS must be four-point averaged over velocity points before it is used.

Vertical mixing will be evaluated precisely as in (79) except now the exchange coefficient at the bottom of the layer is the surface value while at the top it is calculated from Level 2.5. Thus for potential temperature

$$\frac{\theta_{LM}^{n+1}-\theta_{LM}^{n}}{\Delta t_{phy}}=\frac{1}{\rho_{LM}\left(z_{LM-\frac{1}{2}}-z_{sfc}\right)}\left[\left(\rho_{LM-1}+\rho_{LM}\right)KH_{LM-\frac{1}{2}}\left(\frac{\theta_{LM-1}^{n}-\theta_{LM}^{n+1}}{z_{LM-\frac{3}{2}}-z_{sfc}}\right)\right.$$

$$\left.-\left(\rho_{LM}+\rho_{sfc}\right)KHS\left(\frac{\theta_{LM}^{n+1}-\theta_{sfc}^{n}}{z_{LM-\frac{1}{2}}-z_{sfc}}\right)\right] \qquad (91)$$

where ρ_{sfc} is the air density at the surface. For specific humidity, the soil moisture ratio must be included:

$$\frac{q_{LM}^{n+1}-q_{LM}^{n}}{\Delta t_{phy}}=\frac{1}{\rho_{LM}\left(z_{LM-\frac{1}{2}}-z_{sfc}\right)}\left[\left(\rho_{LM-1}+\rho_{LM}\right)KH_{LM-\frac{1}{2}}\left(\frac{q_{LM-1}^{n}-q_{LM}^{n+1}}{z_{LM-\frac{3}{2}}-z_{sfc}}\right)\right.$$

$$\left.-\left(\rho_{LM}+\rho_{sfc}\right)KHS\left(\frac{WET}{WFC}\right)\left(\frac{q_{LM}^{n+1}-q_{sfc}^{n}}{z_{LM-\frac{1}{2}}-z_{sfc}}\right)\right] \qquad (92)$$

The finite difference equations for the u and v components of the wind are identical to (91) except KM and KMS replace KH and KHS. Again the exchange coefficients and air density must be four-point averaged over velocity points.

The solutions for the updated model variables in the lowest layer are then

$$\theta_{LM}^{n+1}=\frac{\rho_{LM}\theta_{LM}^{n}+F1\ \theta_{LM-1}^{n}+F2\ \theta_{sfc}^{n}}{\rho_{LM}+F1+F2} \qquad (93a)$$

$$q_{LM}^{n+1}=\frac{\rho_{LM}q_{LM}^{n}+F1\ q_{LM-1}^{n}+\mu\ F2\ q_{sfc}^{n}}{\rho_{LM}+F1+F2} \qquad (93b)$$

$$u_{LM}^{n+1}=\frac{\bar{\rho}_{LM}^{xy}\ u_{LM}^{n}+F3\ u_{LM-1}^{n}}{\bar{\rho}_{LM}^{xy}+F3+F4} \qquad (93c)$$

$$v_{LM}^{n+1}=\frac{\bar{\rho}_{LM}^{xy}\ v_{LM}^{n}+F3\ v_{LM-1}^{n}}{\bar{\rho}_{LM}^{xy}+F3+F4} \qquad (93d)$$

where

$$F1 = \frac{FS\ KH_{LM-\frac{1}{2}}\ (\rho_{LM-1} + \rho_{LM})}{z_{LM-\frac{3}{2}} - z_{sfc}} \tag{94a}$$

$$F2 = \frac{FS\ KHS\ (\rho_{LM} + \rho_{sfc})}{z_{LM-\frac{1}{2}} - z_{sfc}} \tag{94b}$$

$$F3 = \frac{FS\ \overline{KM}^{xy}_{LM-\frac{1}{2}}\ (\overline{\rho_{LM-1}}^{xy} + \overline{\rho_{LM}}^{xy})}{z_{LM-\frac{3}{2}} - z_{sfc}} \tag{89c}$$

$$F4 = \frac{FS\ \overline{KMS}^{xy}\ (\overline{\rho_{LM}}^{xy} + \overline{\rho_{sfc}}^{xy})}{z_{LM-\frac{1}{2}} - z_{sfc}} \tag{94d}$$

$$F5 = \frac{\Delta t_{phy}}{z_{LM-\frac{1}{2}} - z_{sfc}} \tag{94e}$$

$$\mu = WET / WFC \tag{94f}$$

4.2 Precipitation

Both large scale and convective rainfall are described.

4.2.1 Large Scale Precipitation

The standard rationale is used in calculating this quantity. Condensation is assumed to occur if the relative humidity is greater than 95% and is summed layer by layer downward from the top. If a layer is subsaturated (RH<95%), the water is evaporated until the layer becomes saturated. Corresponding changes in temperature and specific humidity resulting from the phase change are calculated.

4.2.2 Convective Precipitation

The eta model uses the method suggested by Betts (1986) to determine convective rainfall. This approach involves construction of so-called reference profiles of temperature and specific humidity over each relevant height point, then relaxing the ambient profiles toward them. Because the nature of the reference profiles is based on numerous observations, the procedure ensures that the atmosphere will adjust toward a realistic state. The new T and q at each level after adjustment are given by

$$T(new) = T(old) + \frac{\Delta t_{phy}}{\tau}\left[T_{ref} - T(old)\right] \qquad (95a)$$

$$q(new) = q(old) + \frac{\Delta t_{phy}}{\tau}\left[q_{ref} - q(old)\right] \qquad (95b)$$

with τ (=3000 s) being the relaxation time.

Before the routine is used, two lookup tables are generated. One is called PTBL and yields saturation point pressure (PSP) given the potential temperature and specific humidity while the other, TTBL, is of the temperature given the saturation equivalent potential temperature θ_{es} and the pressure. The former table is used to locate cloud base and the latter is used to find temperatures within the cloud. The motivation for using such tables is simply to avoid repeatedly calculating the exponentials needed in the Clausius-Clapeyron equation thereby saving considerable CPU time.

The first step is to determine fundamental characteristics of any convective clouds present. The three lowest model levels above the surface are searched and the one with the greatest θ_{es} is assumed to coincide with cloud base, whereupon, θ, θ_{es}, and PSP (from PTBL) are retained for that level. Knowing θ_{es} and the ambient vertical pressure structure, the temperature of a parcel, as it is lifted moist adiabatically above cloud base, is found (from TTBL). If the parcel temperature is warmer, or fewer than 3°K cooler, than the environment at a given level, then it is considered buoyant and proceeds to move up to the next level. Once the parcel temperature at a level becomes more than 3°K cooler than the environment, the cloud top is chosen as the level below.

The vertical extent of the cloud is the criterion used for choosing the type of convection and thus the nature of the reference profiles. If the cloud rises five or more levels above cloud base, then deep convection will occur. Shallow convection is assumed if the cloud rises ~~three or~~ two four levels. Convection is skipped if a cloud rises fewer than ~~three~~ two levels.

4.2.2.1 Shallow Convection Profiles

Based on observational evidence, Betts concludes that the lapse rate within shallow cumuli is similar to a mixing line derived by mixing air above the capping inversion with that in the subcloud layer. This fact is used to construct a first guess to the reference profiles. For shallow convection, the cloud top is raised one level higher to allow partial mixing above the previously defined cloud top.

Let LTOP and LBOT denote the model levels of cloud top and bottom, respectively. The slope, M, of the mixing line is found from

$$M = \frac{\theta_{LTOP} - \theta_{LBOT}}{PSP_{LTOP} - PSP_{LBOT}} \tag{96}$$

Assuming ~~that the temperature in the two lowest cloud levels will not be changed by the adjustment and~~ that the lapse rate of the reference profile at higher levels is 0.8 times that of the mixing line, then the first guess reference temperature profile below cloud top is given by

$$T^{(1)}_{ref,L} = \left(APE_L\right)^{-1}\left[T^{(1)}_{ref,L+1}\ APE_{L+1} + 0.8\ M\ \left(p_L - p_{L+1}\right)\right] \tag{97}$$

where the superscript (1) refers to the first guess and

$$APE = \left(\frac{10^5}{p_L}\right)^{\kappa}.$$

T_{ref} at the lowest two levels of the cloud are equal to the ambient temperature. The reference temperature for the cloud top is modified for the capping inversion such that

$$T^{(1)}_{ref,LTOP} = \left(APE_{LTOP}\right)^{-1}\left[T^{(1)}_{ref,LTOP+1}\ APE_{LTOP+1}\right.$$
$$\left. + 1.1\left(\frac{PSP_{LTOP+2} - PSP_{LTOP}}{p_{LTOP+1} - p_{LTOP}} - 1\right)(0.8\ M)\left(p_{LTOP} - p_{LTOP+1}\right)\right] \tag{98}$$

The first guess specific humidity profile is determined by choosing a subsaturation pressure value, DSP, which will correspond to the profile. The value currently used is -4000 Pa. Thus at each cloud level above the lowest two, T_{ref} and $p_{sat}(=p_L+DSP)$ are inverted to yield q_{ref}. The formula used to invert these values is that of the saturation specific humidity:

$$q^{(1)}_{ref,L} = \frac{PQ0}{p_{sat,L}}\exp\left[A2\left(\frac{T^{(1)}_{ref,L}\ APE_L - A3\ APE_{sat,L}}{T^{(1)}_{ref,L}\ APE_L - A4\ APE_{sat,L}}\right)\right] \tag{99}$$

where:

$PQ0 = 379.90516$, $A2 = 17.269388$, $A3 = 273.15$, $A4 = 35.86$, and $APE_{sat,L} = \left(\frac{10^5}{p_{sat,L}}\right)^{\kappa}$.

Corrections must now be applied to the first guess profiles to satisfy the constraints

$$\int_{P_{BOT}}^{P_{TOP}} c_p\left(T_{ref} - T\right) dp = 0 \tag{100a}$$

$$\int_{P_{BOT}}^{P_{TOP}} L_v\left(q_{ref} - \bar{q}\right) dp = 0 \tag{100b}$$

where L_v is the latent heat of vaporization. Qualitatively, (100a) and (100b) state that the vertically integrated sensible heat and moist static energy will not change during the adjustment process. Note that (100b) infers that no net condensation/evaporation can occur in a column due to shallow convection. The process simply redistributes heat and moisture vertically. The corrections added to (97), (98), and (99) ~~more than two levels above cloud base~~ to obtain the final profiles are thus

$$\Delta T = \frac{\sum_{L=LBOT}^{LTOP} \left[T_L - T^{(1)}_{ref,L}\right](\Delta\eta)_L}{\sum_{L=LBOT}^{LTOP} (\Delta\eta)_L} \tag{101a}$$

$$\Delta q = \frac{\sum_{L=LBOT}^{LTOP} \left[q_L - q^{(1)}_{ref,L}\right](\Delta\eta)_L}{\sum_{L=LBOT}^{LTOP} (\Delta\eta)_L} \tag{101b}$$

4.2.2.2 Deep Convection Profiles

In constructing the first guess profiles for deep convection, three fundamental points in the cloud are used: the base, the ambient freezing level (L0), and the top. Betts shows that in deep cumuli the lapse rate below the freezing level is slightly less stable than moist adiabatic, i.e., the magnitude of $\partial\theta/\partial p$ along a reference profile is less than $\partial\theta/\partial p$ along the moist adiabat. Above the freezing level, the lapse rate tends back toward the moist adiabat with height.

Let STABD represent the fractional decrease in stability of the first guess temperature reference profile from the moist adiabat below the freezing level. Then for $LBOT > L \geq L0$,

$$T^{(1)}_{ref,L} = \left(APE_L\right)^{-1}\left[T^{(1)}_{ref,L+1}\ \ APE_{L+1} + STABD\left(\theta_{cld,L} - \theta_{cld,L+1}\right)\right] \qquad (102)$$

where STABD is assigned the value of 0.90. At cloud base, the reference temperature equals the ambient temperature. The quantity θ_{cld} is the potential temperature of a parcel lifted along a moist adiabat from cloud base to level L and is derived from TTBL. Above the freezing level, the reference temperature is linearly interpolated between those at the freezing level and cloud top. Thus for L0>L>LTOP

$$T^{(1)}_{ref,L} = \left(APE_L\right)^{-1}\left[\theta_{cld,L} - \left(\frac{p_L - p_{LTOP}}{p_{L0} - p_{LTOP}}\right)\left(\theta_{cld,L0} - T^{(1)}_{ref,L0}\ \ APE_{L0}\right)\right]$$

$$+\left(\frac{p_{L0} - p_L}{p_{L0} - p_{LTOP}}\right)\left(\theta_{cld,LTOP} - \theta_{LTOP}\right)\Big] \qquad (103)$$

In constructing the humidity reference profiles, subsaturation pressure values are assigned to cloud base (DSPB), the freezing level (DSP0), and cloud top (DSPT). The values used in the model are (DSPB, DSP0, DSPT)=(-3000, -2500, -2000) Pa.

$$DSP_L = \frac{\left(p_{L0} - p_L\right)\ DSPT + \left(p_L - p_{LTOP}\right)\ DSP0}{p_{L0} - p_{LTOP}}, \qquad L < L0 \qquad (104a)$$

$$DSP_L = \frac{\left(p_{LBOT} - p_L\right)\ DSP0 + \left(p_L - p_{L0}\right)\ DSPB}{p_{LBOT} - p_{L0}}, \qquad L \geq L0 \qquad (104b)$$

In the special case that the freezing level is fewer than three model levels above cloud base, then DSP=-3000 Pa throughout the cloud. The first guess humidity reference values $q^{(1)}_{ref}$ are now determined by inverting $T^{(1)}_{ref}$ and $p_{ref}(=p_L+DSP)$.

The energy constraint used in correcting the first guess profiles for deep convection is that total enthalpy, $H = c_p T + L_v q$, will be conserved in the vertical through the adjustment process, i.e.,

$$\int_{p_{BOT}}^{p_{TOP}} \left(H_{ref} - H\right) dp = 0 \qquad (105)$$

The correction that must be made to the first guess reference profile enthalpies so that (105) will hold is then

$$\Delta H = \frac{\sum_{L=LTOP}^{LBOT} \left[c_p \left(T_L - T_{ref,L}^{(1)} \right) + L_v \left(q_L - q_{ref,L}^{(1)} \right) \right] (\Delta\eta)_L}{\sum_{L=LTOP}^{LBOT} (\Delta\eta)_L} \qquad (106)$$

No correction will be applied to the cloud top and thus the q field there will ultimately be changed only by the first guess q profile. This is done to avoid systematic corrections at levels just below the tropopause.

At every level below cloud top, the first guess temperature profile is corrected. The size of the correction is found as follows. Consider the definition of the total differential of the enthalpy:

$$dH = \frac{\partial H}{\partial T} dT + \frac{\partial H}{\partial p} dp \qquad (107)$$

Since the adjustment occurs at a given η level, the process is isobaric and the second term on the right hand side of (107) is zero. The partial derivative of enthalpy with respect to temperature is

$$\frac{\partial H}{\partial T} = c_p + L_v \frac{\partial q_{sat}}{\partial T} \qquad (108)$$

and the resulting derivative of q_{sat} is obtained by differentiating (99) which gives

$$\frac{\partial q_{sat}}{\partial T} = \frac{A2(A3 - A4) q_{sat,L}}{\left(T_{ref,L}^{(1)} - A4 \right)^2} \qquad (109)$$

Approximating dT in (107) by

$$\Delta T = T_{ref}^{(2)} - T_{ref}^{(1)}$$

, then solving for $T_{ref}^{(2)}$ yields

$$T_{ref,L}^{(2)} = T_{ref,L}^{(1)} + \frac{\Delta H}{c_p + L_v \left(\frac{\partial q_{sat}}{\partial T} \right)_L} \qquad (110)$$

where ΔH is taken from (106).

Subsaturation values remain constant for the enthalpy correction thus p_{sat} is unchanged from the first guess. The corrected reference humidity is therefore given by

$$q_{ref,L}^{(2)} = \left(\frac{PQ0}{p_{sat,L}} \right) \exp \left[A2 \left(\frac{T_{ref,L}^{(2)} \; APE_L - A3 \; APE_{sat,L}}{T_{ref,L}^{(2)} \; APE_L - A4 \; APE_{sat,L}} \right) \right] \qquad (111)$$

4.2.2.3 Adjustment and Precipitation

To approximate the effects of convection, the model values of T and q are relaxed toward the reference profiles according to (95). The changes in T and q that should occur during adjustment are thus

$$(\Delta T)_L = \left(T^{(2)}_{ref,L} - T_L\right)/\tau \qquad (112a)$$

$$(\Delta q)_L = \left(q^{(2)}_{ref,L} - q_L\right)/\tau \qquad (112b)$$

Before these changes are added to the old values, though, they are smoothed horizontally so that

$$(\Delta T)'_L = 1/8\left\{\delta^2_x(\Delta T_L) + \delta^2_y(\Delta T_L)\right\} + \Delta T_L \qquad (113a)$$

$$(\Delta q)'_L = 1/8\left\{\delta^2_x(\Delta q_L) + \delta^2_y(\Delta q_L)\right\} + \Delta q_L \qquad (113b)$$

The precipitation P over a grid box formed as a result of the adjustment can be inferred from (106):

$$P = \int_{p_{BOT}}^{p_{TOP}} \left[\frac{q^{(2)}_{ref,L} - q_L}{\tau}\right]\frac{dp}{g} \qquad (114a)$$

$$= -\left(\frac{c_p}{L_v}\right)\int_{p_{BOT}}^{p_{TOP}} \left[\frac{T^{(2)}_{ref,L} - T_L}{\tau}\right]\frac{dp}{g} \qquad (114b)$$

Letting $CPRLG = \dfrac{c_p}{\rho_w g L_v}$ where $\rho_w = 10^3 kg\,m^{-3}$, then

the convective rainfall occurring during one time step is calculated by

$$P = \sum_{L=LTOP}^{LBOT} CPRLG\left(\frac{T^{(2)}_{ref,L} - T_L}{\tau}\right) PDSL\,(\Delta\eta)_L \qquad (115)$$

Δt_{PHY}

4.3 Ground Processes

The model's simulation of surface processes includes the calculation of surface temperature, specific humidity, and the accumulation/loss of water. Qualitatively, the energy balance ($Jm^{-2}s^{-1}$) is given by

$$\rho_s c_s d_s \frac{\theta_{sfc}^{n+1} - \theta_{sfc}^{n}}{\Delta t_{phy}} = FGF\left(R_{\downarrow} - R^{\uparrow}\right) + \rho_a c_p KHS\left(\frac{\theta_{LM}^{n+1} - \theta_{sfc}^{n+1}}{\Delta z_a}\right) - \rho_g c_g K_g\left(\frac{\theta_{sfc}^{n+1} - \theta_g}{\Delta z_g}\right)$$

$$+ APE_{sfc}^{n+1}\ \mu\rho_a L_v KHS\left(\frac{q_{LM}^{n+1} - q_{sat}\left(\theta_{sfc}^{n+1}\right)}{\Delta z_a}\right) \qquad (116)$$

The incoming radiation $R\downarrow$ is taken from the radiation routine while the outgoing radiation $R\uparrow$ is given by

$$\epsilon\sigma\left(\frac{\theta_{sfc}^{n+1}}{APE_{sfc}}\right)^4,$$

where ϵ is the emissivity (1.0 over soil, 0.4 over water substance), σ is the Stefan-Boltzmann constant,

$$\sigma = 5.67 \times 10^{-8} Jm^{-2}K^{-4}s^{-1},$$

, FGF is a correction to the net radiative flux (0.68 if $R_{net}>0$, 0.81 if $R_{net}<0$; from Nickerson and Smiley (1975));

$APE_{sfc} = \left(10^5/p\right)^{\kappa}$, $\rho_s = \rho_g$ is the soil density , $1500 kgm^{-3}$.

$c_s = c_g$ is the specific heat of soil, $1339.2 Jkg^{-1}K^{-1}$; d_s is the surface layer depth (0.1 m).

Δz_g is the depth of the underground layer (2.5 m);
Δz_a is the height of the lowest midlayer predictive surface above the ground (the denominator of Eq.(79c)).
θ_{LM} and q_{LM} are the potential temperature and specific humidity at that level;
θ_g is an underground potential temperature which is a function of geographic latitude and surface elevation (see Eq.(9)).
K_g is the exchange coefficient between the surface and underground layers ($5\times10^{-7}m^2/s$) .
μ is the ratio of soil moisture to maximum soil moisture allowed (0.1125 m) which always equals 1 over sea, ice, and snow.
L_v is the latent heat of vaporization.
Over snow and sea ice $\rho_g = 916.6 kgm^{-3}$, $c_g = 2060 J/(kgK)$, and $K_g = 1.0755\times10^{-6}m^2/s$.

In order to isolate θ_{sfc}^{n+1}, Eq. (116) must be linearized by using a simple approximation obtained from the first two terms of the Taylor expansion:

$$\left(\theta_{sfc}^{n+\Delta n}\right)^4 \cong \left(\theta_{sfc}^{n}\right)^4 + 4(\Delta n)\left(\theta_{sfc}^{n}\right)^3\left(\frac{\partial\theta_{sfc}}{\partial n}\right) \qquad (117)$$

With $\Delta n = 1$ time step and $\frac{\partial \theta_{sfc}}{\partial n} \simeq \frac{\theta_{sfc}^{n+1} - \theta_{sfc}^{n}}{\Delta n}$,

$$\left(\theta_{sfc}^{n+1}\right)^4 = 4\left(\theta_{sfc}^{n}\right)^3 \theta_{sfc}^{n+1} - 3\left(\theta_{sfc}^{n}\right)^4 \tag{118}$$

Likewise, the saturation specific humidity at the ground is

$$q_{sat}\left(\theta_{sfc}^{n+1}\right) \simeq q_{sat}\left(\theta_{sfc}^{n}\right) + \Delta\theta_{sfc} \frac{\partial q_{sat}}{\partial \theta} \tag{119}$$

Taking $\frac{\partial q_{sat}}{\partial \theta}$ from (109) and with $\Delta\theta_{sfc} = \theta_{sfc}^{n+1} - \theta_{sfc}^{n}$, then

$$q_{sat}\left(\theta_{sfc}^{n+1}\right) = q_{sat}\left(\theta_{sfc}^{n}\right)\left\{1 + \frac{A2\ \ APE_{sfc}^{n+1}\ \ (A3 - A4)\left(\theta_{sfc}^{n+1} - \theta_{sfc}^{n}\right)}{\left(\theta_{sfc}^{n} - A4\ \ APE_{sfc}^{n+1}\right)^2}\right\} \tag{120}$$

Inserting (118) and (120) into (116) and solving for θ_{sfc}^{n+1} yields

$$\theta_{sfc}^{n+1} = X1 / X2 \tag{121a}$$

$$X1 = \Delta t_{phy}\{FFS\ \ \theta_{LM}^{n+1} + GFFC\ \ \theta_g + QFC1\ \left[q_{LM}^{n+1} - q_{sat}\left(\theta_{sfc}^{n}\right)\left(1 - QFC2\ \ \theta_{sfc}^{n}\right)\right]$$

$$+ FGF\ \left[R\downarrow + 3\epsilon\sigma\left(T_{sfc}^{n}\right)^3 \theta_{sfc}^{n}\right]\} + \rho_s c_s d_s \tag{121b}$$

$$X2 = \rho_s c_s d_s + \Delta t_{phy}\left\{FFS + GFFC + QFC2\ \ q_{sat}\left(\theta_{sfc}^{n}\right)\ \ QFC1 + RADFC\right\} \tag{121c}$$

where

$$FFS = c_p \rho_{LM}^{n+1}\ \ KHS / \Delta z_a \tag{122a}$$

$$GFFC = c_g \rho_g K_g / \Delta z_g \tag{122b}$$

$$QFC1 = \mu \rho_{LM}^{n+1} L_v\ \ KHS\ \ APE_{sfc}^{n+1} / \Delta z_a \tag{122c}$$

$$QFC2 = \frac{A2(A3 - A4)\ \ APE_{sfc}^{n+1}}{\theta_{sfc}^{n} - A4\ \ APE_{sfc}^{n+1}} \tag{122d}$$

$$RADFC = 4\epsilon\sigma\left(T_{sfc}^{n}\right)^3\ \ FGF \tag{122e}$$

Eq.(121) is used only over land and sea ice points. The surface potential temperature is constant over open ocean. Given θ_{sfc}, the saturation specific humidity can be calculated for use in finding the moisture exchange. The value of q_{sfc} uses the formula in (99):

$$q_{sfc}^{n} = \frac{PQ0}{p_{sfc}^{n}} \exp\left\{A2\left(\frac{\theta_{sfc}^{n} - A3\ \ APE_{sfc}^{n}}{\theta_{sfc}^{n} - A4\ \ APE_{sfc}^{n}}\right)\right\} \tag{123}$$

5 Horizontal Boundary Conditions

The integration domain of the eta model excludes the two outermost rows of the horizontal grid as seen in Fig. 7. Pressure, temperature, and relative humidity (from which specific humidity is inferred) as well as the wind components are taken from the aviation run of the global spectral model for the initial time and for every six hours of the forecast. These data on mandatory pressure levels are interpolated vertically to the eta predictive surfaces as described in Section 2.4 and horizontally to the E grid using bilinear interpolation. Only those values along the outermost row of the grid are retained. The tendencies of the forecast quantities are obtained by assuming linear change during each six-hour period and are applied to the values of the outer row after every adjustment time step during the integration.

After each update of the outer row, the wind components normal to the boundary are checked except at the eight velocity points nearest the four corners (boxed V's in Fig. 7). If the normal component is outward, the tangential component is replaced by a linear extrapolation of the first two similar components inside the integration domain. For example, consider the wind at (2,1) in Fig. 7. If the v component is negative (outward) then the u component is reassigned a value of 2 u(2,3) - u(2,5). This is done to avoid over-specification of the boundary wind.

The second row within the outer boundary is a blend of the outer row and the third row inside which is included in the integration. The quantities PD (pressure difference between the surface and the top of the domain), T, and q are updated after each Δt_{adj} at the height points of the second row by simple four-point averaging, e.g.,

$$T(1,2) = .25[T(1,1) + T(2,1) + T(1,3) + T(2,3)].$$

The wind components are updated by the same four-point averaging at all but the four circled velocity points ~~in the second row~~. At the circled locations, a six-point weighted average is used. Specifically, the u components at the noted points on the southern side are given by

$$u(2,2) = (4/15)\,[u(1,1) + u(2,1) + u(2,3)] + (1/15)\,[u(1,2) + u(1,4) + u(2,4)] \qquad (131a)$$

$$u(IM-1,2) = (4/15)\,[u(IM-1,1) + u(IM-2,1) + u(IM-2,3)] + (1/15)\,[u(IM,2) + u(IM,4) + u(IM-1,4)] \qquad (131b)$$

The components are updated at these four points prior to those at the other velocity points in the second row.

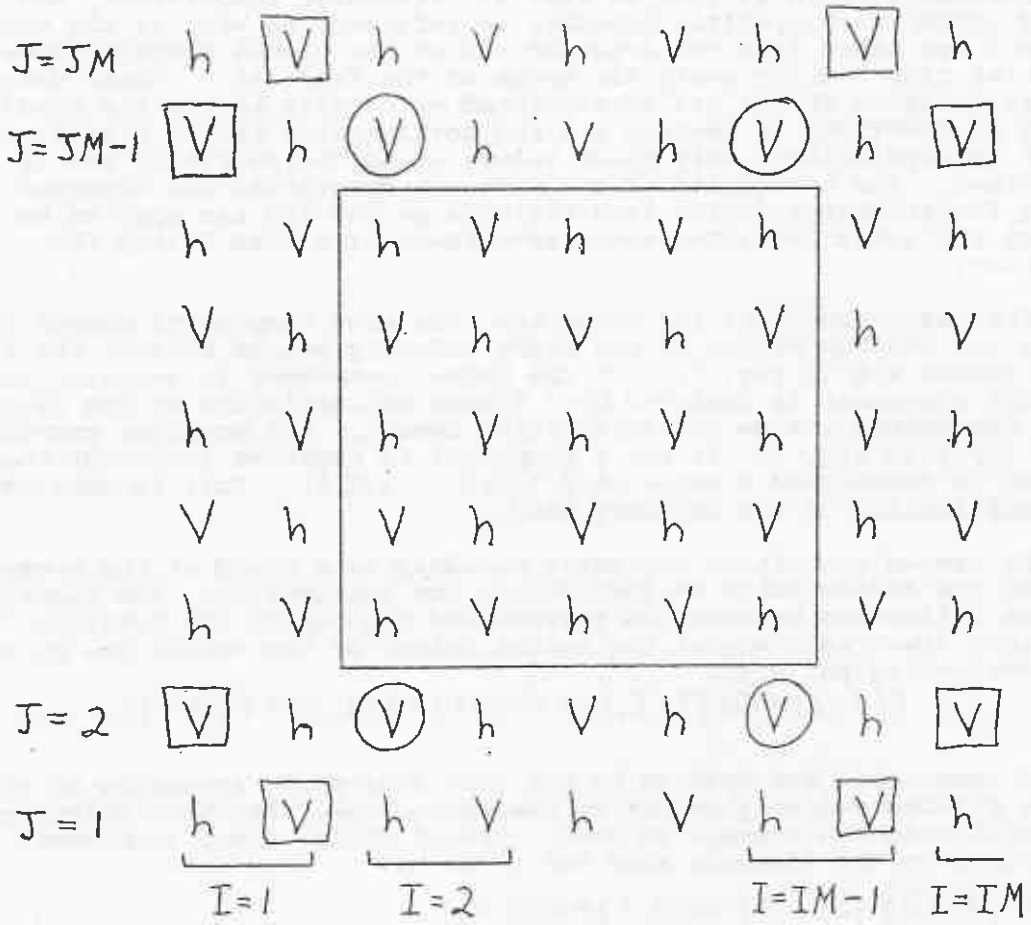

Fig. 7. The eta model's E grid with solid line enclosing the integration domain. Boxed and circled V's are handled differently than others in boundary region; see text.

6 Comparative Results

The resolution and extent of the domain in the horizontal was originally chosen so that the computational effort would be roughly comparable to the Nested Grid Model's. A brief sample of results will be presented.

An example of the interaction of internal processes in the model is seen in Fig. 8 where turbulent exchange coefficients of heat are displayed at 12-h intervals through a 48-h forecast during July 1987. The vertical cross section extends from the northern Gulf of Mexico to northern Ontario. The effect of diurnal surface heating on the growth and decay of mixing in the lower atmosphere is clear. Maximum values of 100 m^2/s over sunny land areas are in good agreement with values given by Mellor and Yamada (1974).

Several sequences of consecutive forecasts have been generated to begin to determine biases that may exist in the model. Fig. 9 shows mean height errors for fourteen forecasts in August 1987. These values are typical of what has been seen in the eta model as well as in the NGM before the latter's errors were reduced through a non-dynamical procedure. The eta model showed a maximum error of -20 gpm around 12 hours then little change thereafter; the sigma version forecast was somewhat similar but the negative errors were about 50% larger. The NGM showed steady and continual cooling resulting in a maximum height error of -60 gpm at 48 hours in the stratosphere.

The precipitation scores indicate that the NGM's rainfall forecasts were superior to those of the eta model during this period. As with subsequent sequences in October and November 1987, the eta model produced higher scores for amounts around 0.50" and greater than 1" while the NGM forecasts produced higher scores for most other amounts.

As examples of specific forecasts from the eta model, two storms which developed over the U.S. during early 1988 will be considered. The surface analysis for 00Z 20 January in Fig. 10a shows a low pressure area over the central Midwest with a 999 mb center in eastern Kansas and a 996 mb center in western Illinois. The 36-h NGM forecast for sea level pressure verifying at this time (Fig. 10b) shows one low in northern Missouri between the two actual centers and another in extreme southeast Arkansas. The eta model forecast (Fig. 10c) produced two centers aligned roughly east-west as observed; the western low was several millibars too deep because the forecast was several hours slow. In subsequent hours of the eta forecast, the western low filled and the eastern low intensified as it moved northeastward which is what occurred in nature.

The verifying and forecast 24-h precipitation totals for the first 24 hours of this forecast are seen in Fig. 11. A line of maxima running northwest-southeast from Nebraska to Georgia was observed. The NGM produced a maximum in Nebraska and a narrow region of slightly heavier rainfall along the Gulf Coast. In contrast, the eta model forecast shows a northwest-southeast line of maxima from Nebraska but the center in Georgia was missed. The NGM won the 0.01" threat and bias scores and the 0.25" bias while the eta model won the 0.25" threat and all other scores for 0.50", 0.75", and 1.00".

During the second 24 hours of this forecast, rainfall was widespread over the eastern Mississippi and Ohio Valleys with two maxima of 60 mm in Tennessee (Fig. 12a). The NGM produced an elongated maximum of 40 mm from northwest Alabama to northern Kentucky. The eta model produced a somewhat rounder area with a maximum of 70 mm over northwest Kentucky. In the scores, the NGM won both 0.01" scores and the 0.25" threat. The eta model tied the NGM for the 0.25" bias and won all other categories through 2.50".

The next major storm to affect the U.S. occurred about 3 weeks later along the east coast. Fig. 13 shows the sea level pressure analysis and forecasts for 12Z 12 February 1988. The analysis shows a complex low pressure system with centers in western New York, Delaware, western Virginia, and northeast of Cape Hatteras. The 48-h NGM forecast placed a low over Detroit with a trough extending southeastward to another low in southern North Carolina. The 48-h eta forecast succeeded in indicating the quadruple structure of the system by placing a low in western New York and another out to sea east of Delaware. A trough existed to the southwest across Virginia and North Carolina and another trough occurred on the southeast side of the system associated with the front trailing from the observed Hatteras low. Most of the precipitation fell during the 24 hours preceding this verification time. The NGM won the 0.25" and 0.75" bias while the eta model won both threat and bias for 0.01" and 0.50" as well as the 0.25" threat.

Experiments have also been carried out to determine how much improvement can be achieved by increasing the horizontal resolution. The severe storm outbreak of 28-29 March 1984 offered an excellent opportunity for such a test since models had largely failed to properly simulate the rather complex cyclogenesis. Fig. 14 shows the paths of the numerous tornadoes which occurred across the Carolinas.

The original low had formed over Texas on 27 March and propagated northeastward. As it crossed the Appalachians, the system split and formed multiple centers. By 00Z 29 March two lows existed, one over West Virginia and another on the North and South Carolina border associated with the severe weather (see Fig. 15a). The 24-h eta model forecast using standard resolution (Fig. 15b) shows a single low over West Virginia with some extension of a trough to the south. Other models had also been unable to produce the southern low. Fig. 15c shows the 24-h eta forecast in which the horizontal resolution was doubled. A separate low center is now clearly indicated in northwest South Carolina near the one that verified.

The observed and predicted precipitation occurring between 12Z 28 March and 12Z 29 March are seen in Fig. 16. Note the three separate bands which verified: along the Ohio Valley, across Kentucky, and across northern Georgia and the Carolinas. The standard resolution forecast produced the central band while only a hint of the southern band which accompanied the severe weather was indicated in North Carolina. However, in the double resolution forecast a very prominent band is seen extending along an axis between Georgia and the Carolinas nearly coincident with that observed.

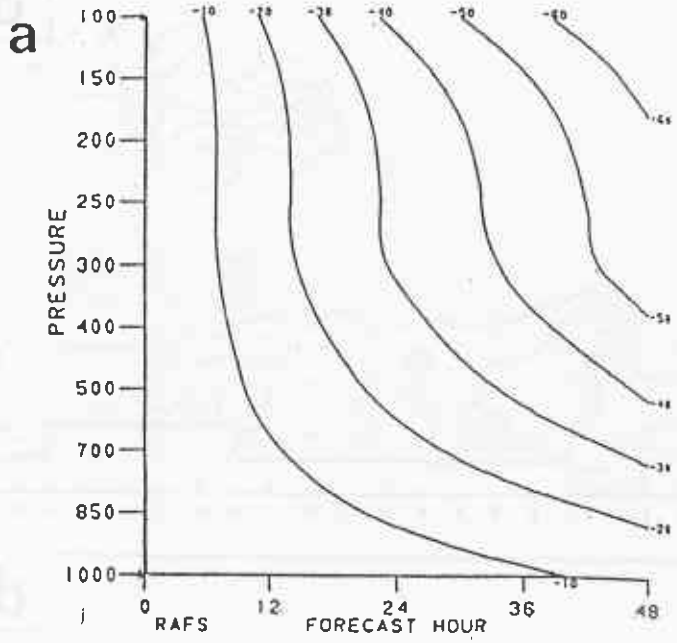

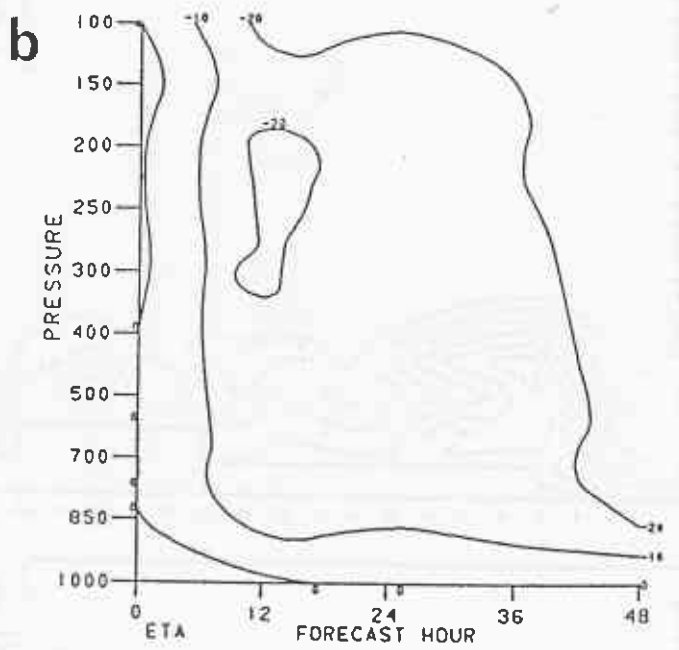

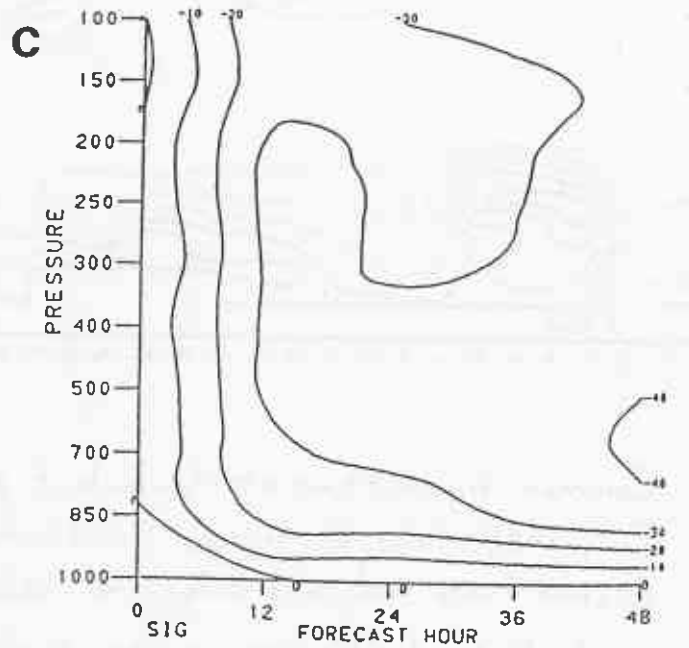

Fig. 9. Mean height errors (m) for 20-26 August 1987 including both 00Z and 12Z cycles: (a) NGM; (b) eta model; (c) sigma mode of eta model.

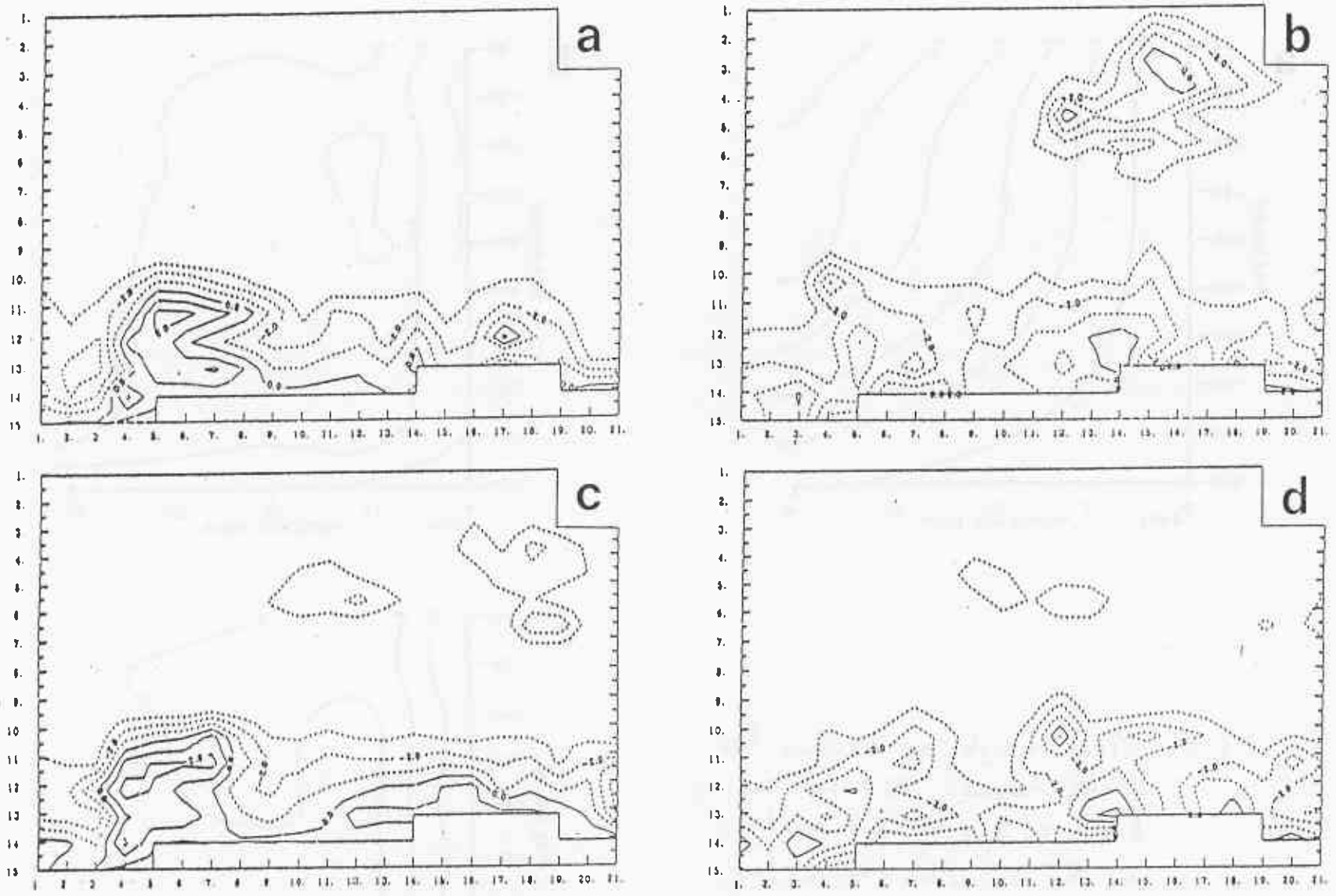

Fig. 8. Common logarithms of turbulent exchange coefficients during 2-day forecast in July 1987: (a) 12-h forecast; (b) 24-h forecast; (c) 36-h forecast; (d) 48-h forecast. Dashed lines indicate negative values. Parts (a) and (c) are in the late afternoon; parts (b) and (d) are in the early morning.

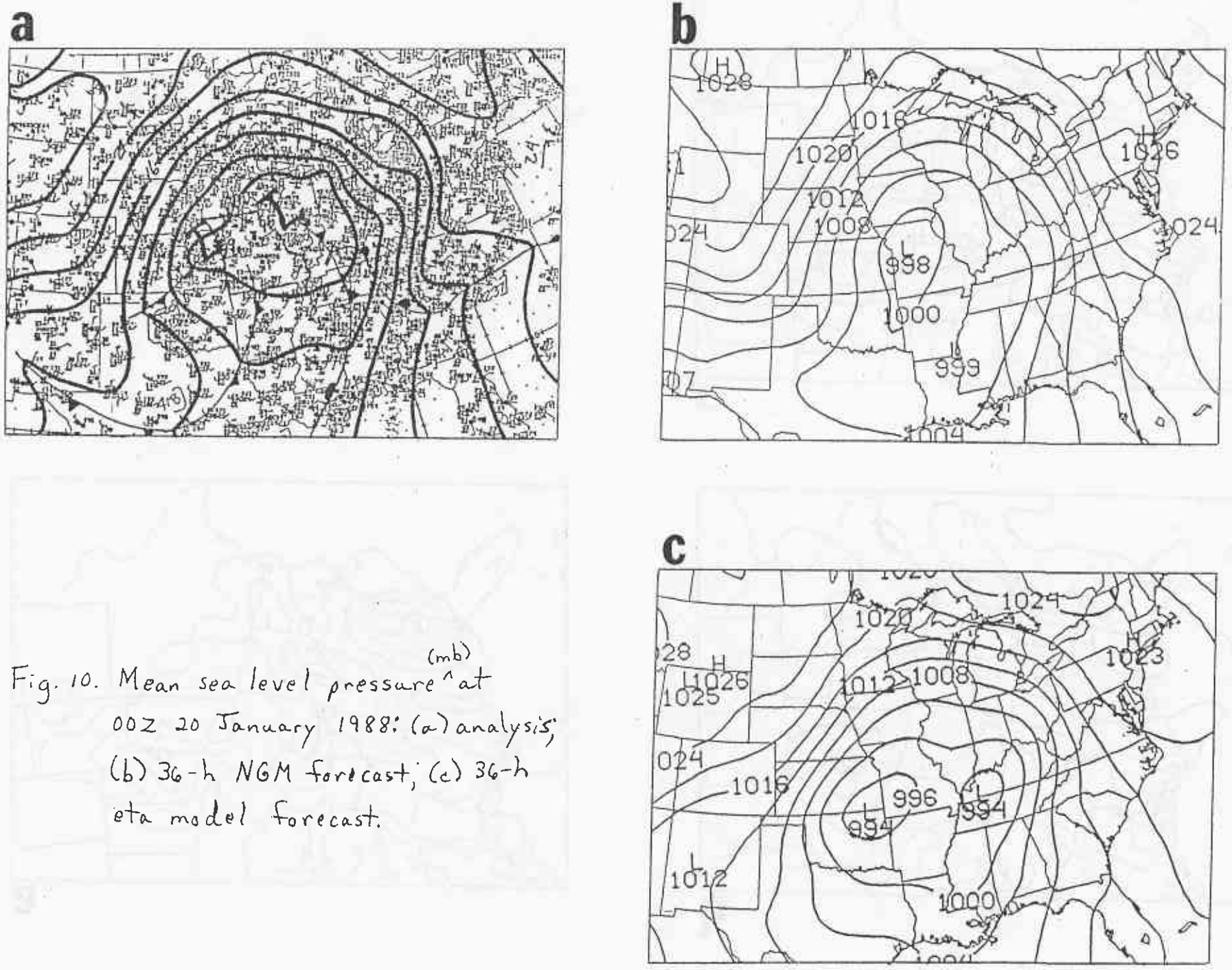

Fig. 10. Mean sea level pressure (mb) at 00Z 20 January 1988: (a) analysis; (b) 36-h NGM forecast; (c) 36-h eta model forecast.

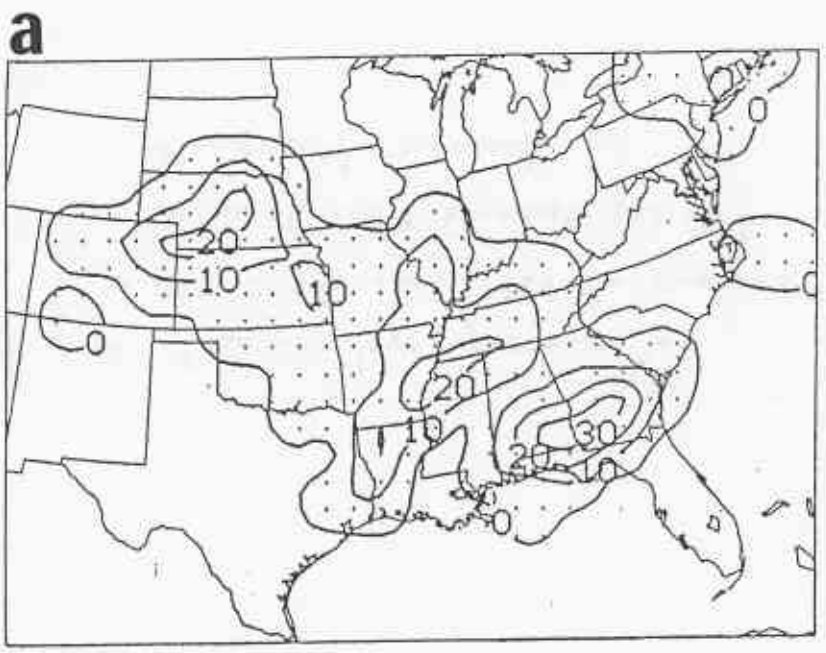

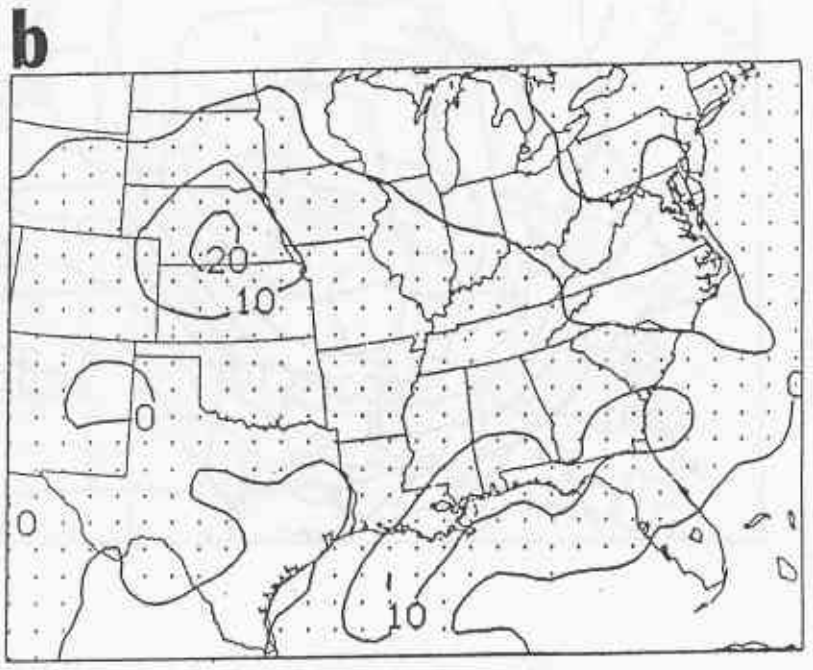

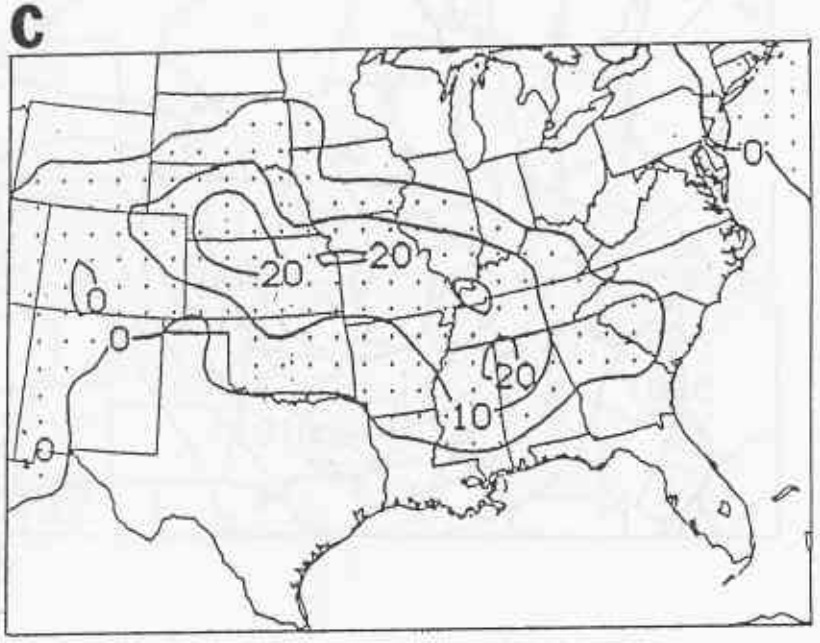

Fig. 11. Cumulative precipitation (mm) for 24-h period ending 12Z 19 January 1988: (a) observed; (b) NGM forecast; (c) eta model forecast. Models initialized at 12Z 18 January.

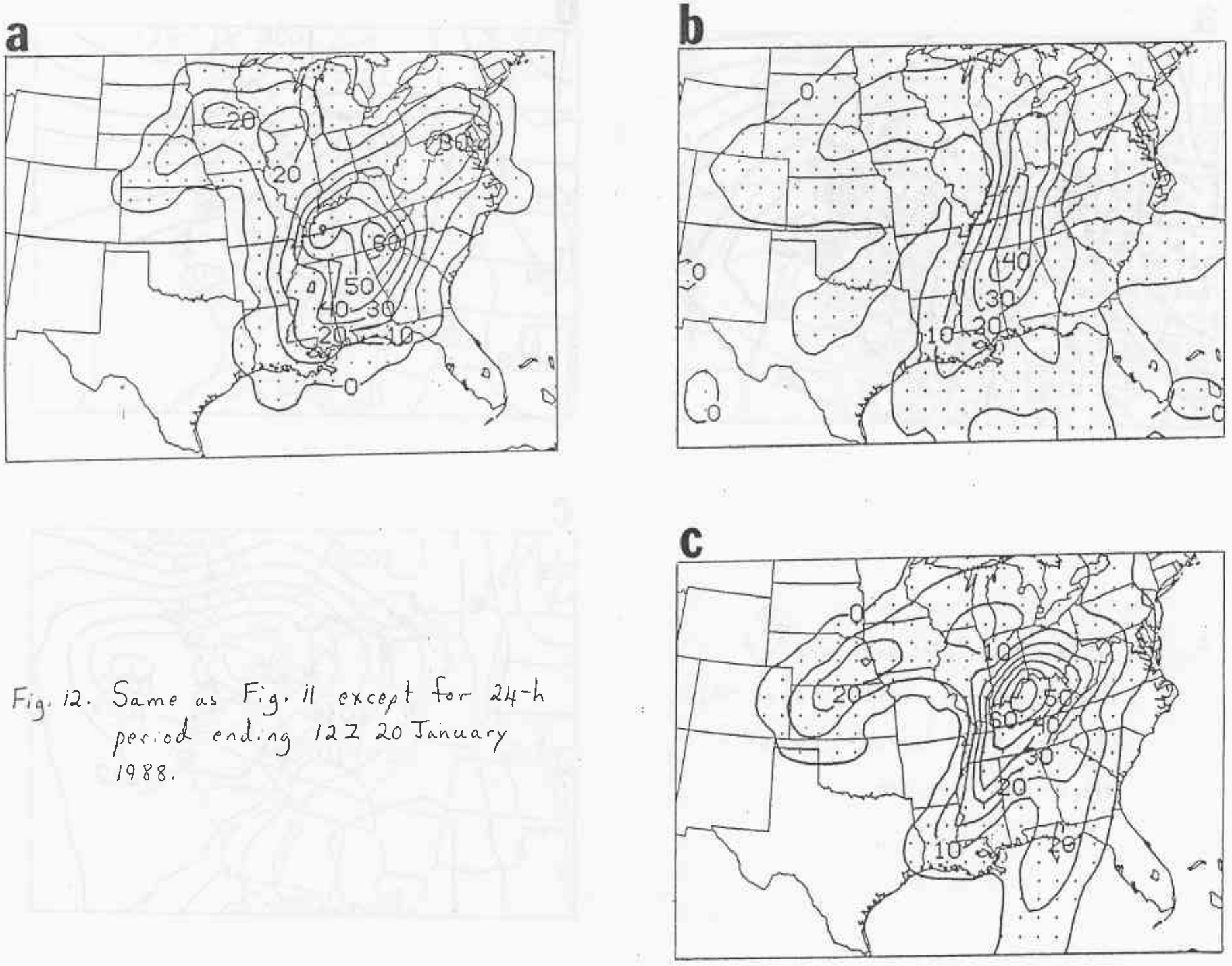

Fig. 12. Same as Fig. 11 except for 24-h period ending 12Z 20 January 1988.

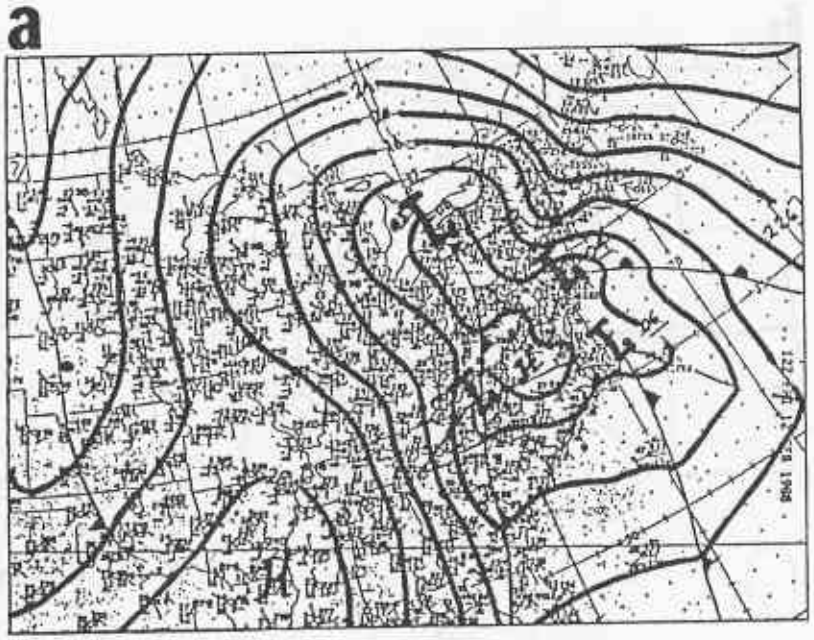

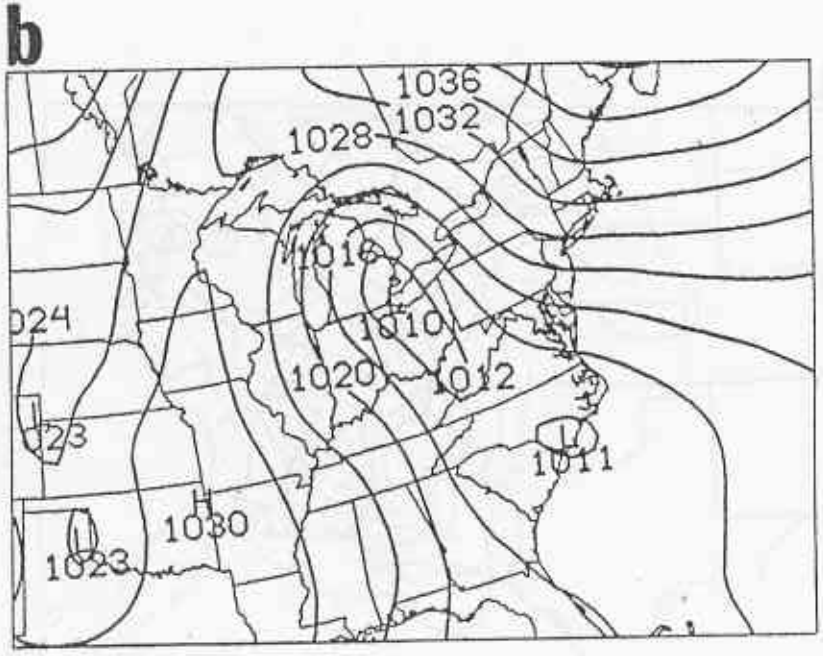

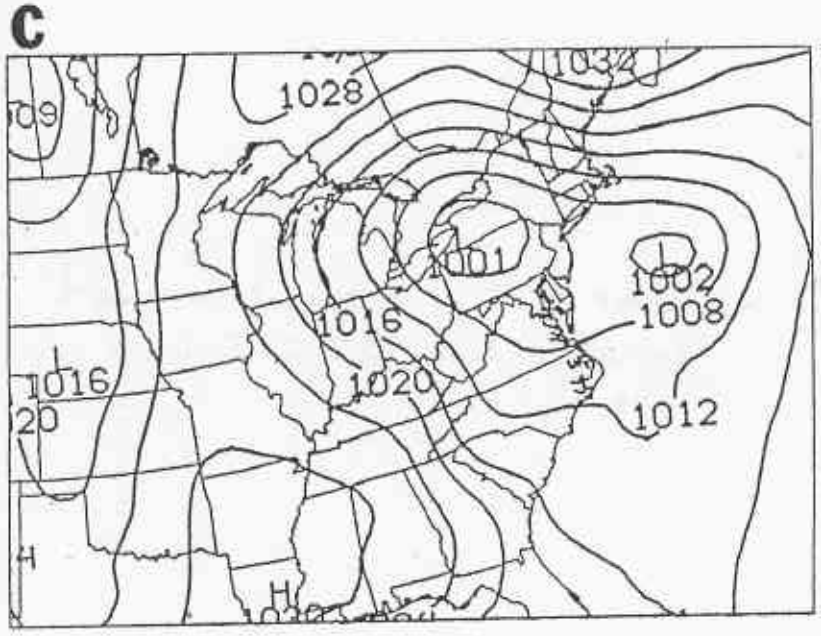

Fig. 13. Mean sea level pressure (mb) at 12Z 12 February 1988: (a) analysis; (b) 48-h NGM forecast; (c) 48-h eta model forecast.

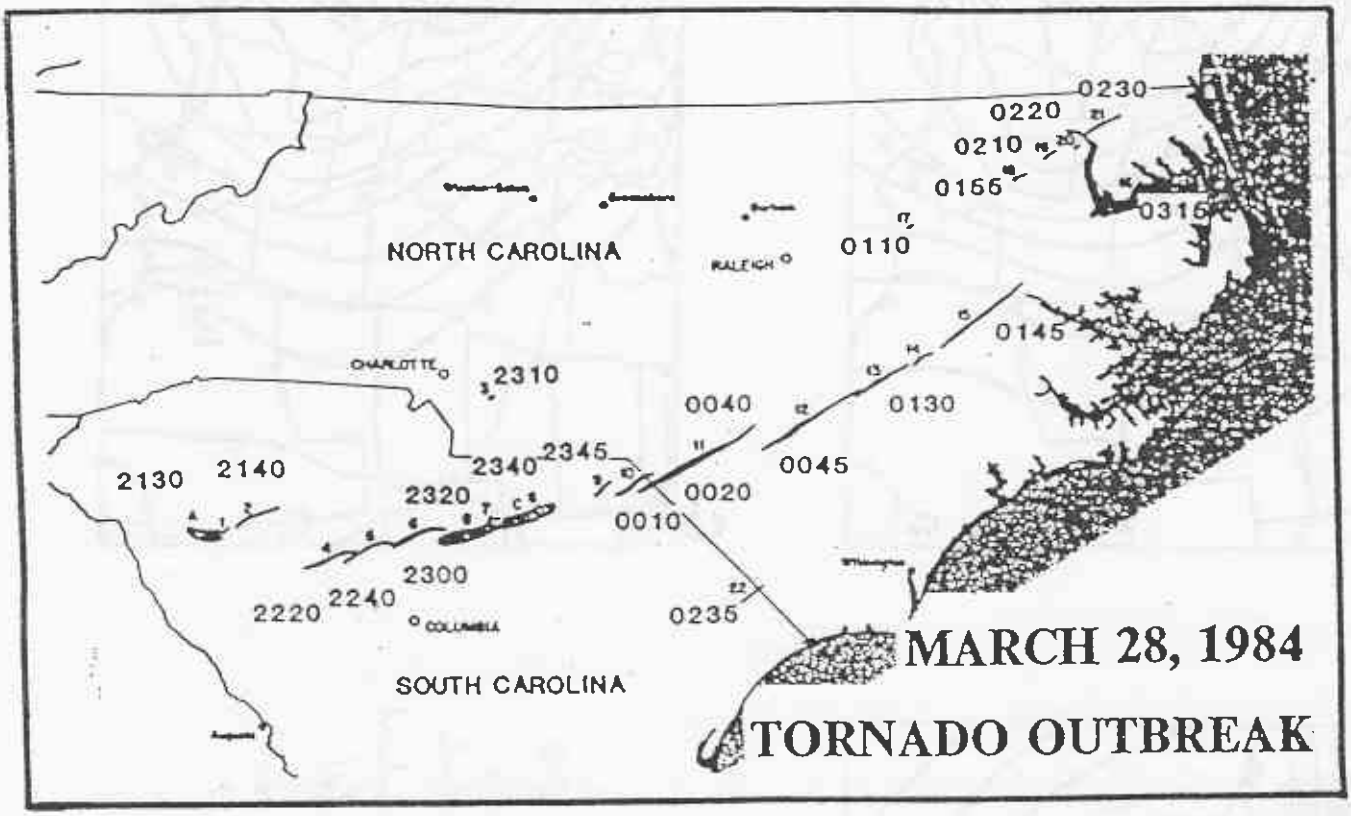

Fig. 14. Tornado paths and times of occurrences (GMT) (from March 1984 Storm Data) between 2100 GMT 28 March 1984 and 0300 GMT 29 March 1984.

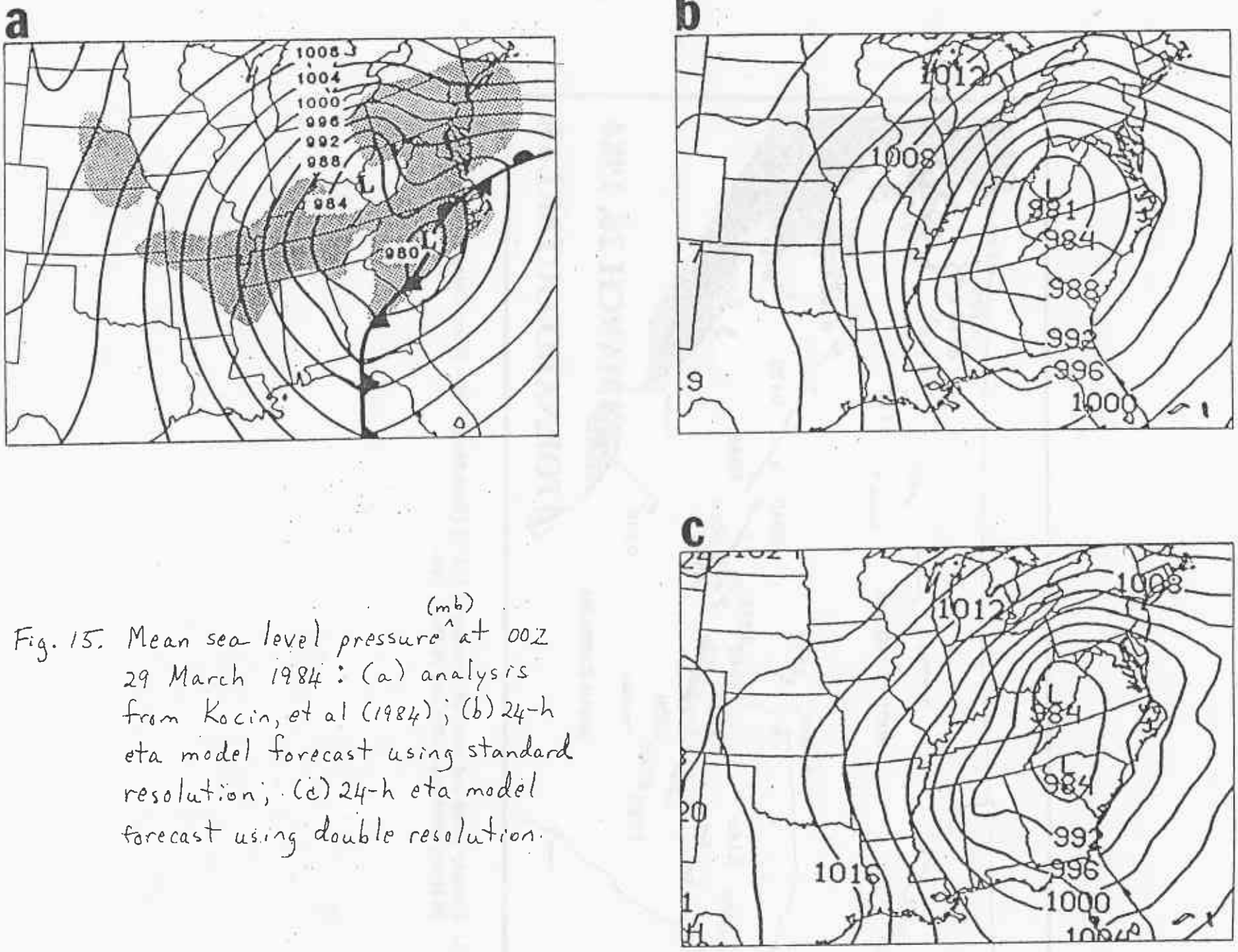

Fig. 15. Mean sea level pressure (mb) at 00Z 29 March 1984: (a) analysis from Kocin, et al (1984); (b) 24-h eta model forecast using standard resolution; (c) 24-h eta model forecast using double resolution.

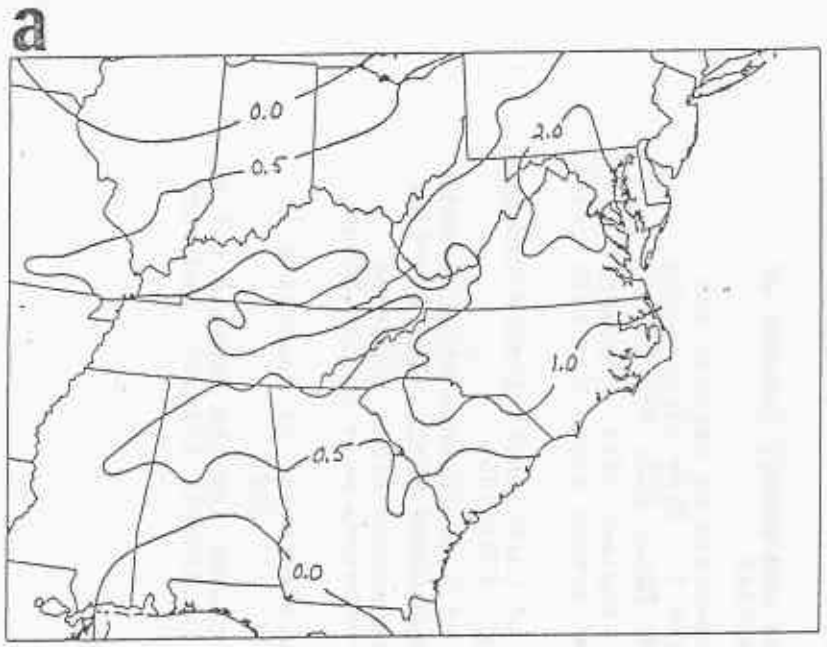

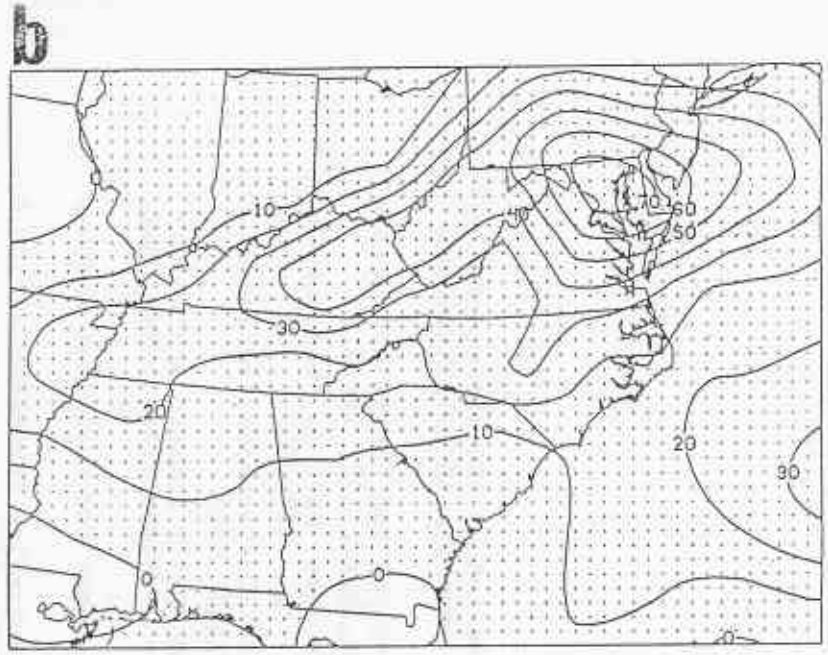

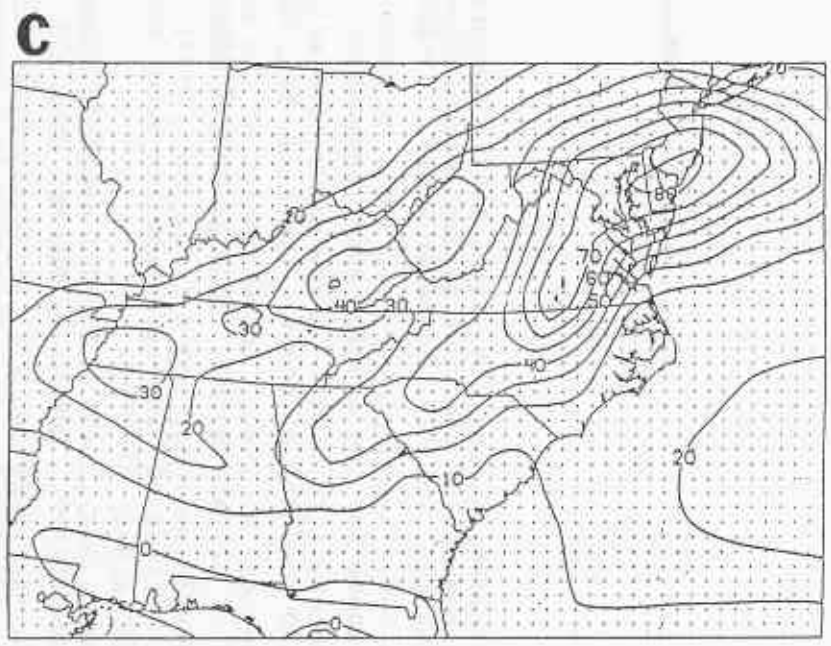

Fig. 16. Cumulative precipitation for 24-h period ending 12Z 29 March 1984: (a) observed; (b) eta model forecast using standard resolution; (c) eta model forecast using double resolution. Units are inches in (a) and millimeters in (b) and (c).

7 References

Arakawa, A. and V.R. Lamb, 1977: Computational design of the basic dynamical processes of the UCLA general circulation model. Methods in Computational Physics, Vol. 17, Academic Press, 173-265.

---------- and --------, 1981: A potential enstrophy and energy conserving scheme for the shallow water equations. Mon. Wea. Rev., 109, 18-36.

Betts, A.K., 1986: A new convective adjustment scheme. Part I: Observational and theoretical basis. Quart. J. Roy. Met. Soc. 112, 667-691.

Davies, R. 1982: Documentation of the Solar Radiation Parameterization in the GLAS Climate Model. NASA Technical Memorandum 83961, 57pp

Dragosavac, M., and Z.I. Janjic, 1987: Topographically induced stationary solutions of linearized shallow water equations on various grids. Mon. Wea. Rev., 115, 730-736.

Gadd, A.J., 1978: A split explicit integration scheme for numerical weather prediction. Quart. J. Roy Met Soc, 104, 569-582.

Harshvardhan and T.G. Corsetti, 1984: Longwave Radiative Parameterization for the UCLA/GLAS GCM. NASA Technical Memorandum 86072, 48pp

Janjic, Z.I. , 1977: Pressure gradient force and advection scheme used for forecasting with steep and small scale topography. Beit. Phys. Atmos. , 50, 186-189.

----------, 1979: Forward-backward scheme modified to prevent two-grid-interval noise and its application in sigma coordinate models. Contrib. Atmos. Phys., 52, 69-84.

----------, 1984: Nonlinear advection schemes and energy cascade on semi-staggered grids. Mon. Wea. Rev., 112, 1234-1245.

Johnson, D. R., and L.W. Uccellini, 1983: A comparison of methods for computing sigma coordinate pressure gradient force for flow over sloped terrain in a hybrid theta-sigma model. Mon. Wea. Rev., 111, 870-886.

Kocin, P.J., L.W. Uccellini, J.W. Zack, and M.L. Kaplan, 1984: Recent examples of mesoscale forecasts of severe weather events along the east coast. NASA Technical Memorandum 86172, 57pp

Mellor, G.L., and T. Yamada, 1974: A hierarchy of turbulence closure models for planetary boundary layers. J. Atmos. Sci. 31, 1791-1806.

---------- and ---------, 1982: Development of a turbulence closure model for geophysical fluid problems. Rev. Geophys. and Space Phys., 20, 851-875.

Mesinger, F., 1973: A method for construction of second-order accuracy difference schemes permitting no false two-grid-interval wave in the height field. Tellus, 25, 444-458.

----------, 1984: A blocking technique for representation of mountains in atmospheric models. Riv. Meteor. Aeronautica, 44, 195-202.

--------- and Z.I. Janjic, 1987: Numerical techniques for the representation of mountains. Observing, Theory and Modeling of Orographic Effects, Seminar 1986, ECMWF, Reading, UK.

If any area is covered by snow or sea ice and (121) yields a surface temperature above freezing, then θ_{sfc} is set to 273.15 APE_{sfc} and q_{sfc} is simply $PQ0/p_{sfc}$. The new θ_{sfc} produces a new $R\uparrow$ of

$$R\uparrow = \epsilon\sigma\left(\frac{\theta_{sfc}}{APE_{sfc}}\right)^4$$

The amount of snow/ice melted (SMELT) is obtained from the heat balance and is given by

$$SMELT = \frac{\Delta t_{phy}}{\rho_w L_f \ APE_{sfc}}[(\theta_{LM}-\theta_{sfc})\ FFS-(\theta_{sfc}-\theta_g)\ GFFC$$

$$+(q_{LM}-q_{sfc})\ QFC1+R\downarrow -R\uparrow] \qquad (124)$$

where L_f is the latent heat of fusion. Any snow occurring over land is allowed to evaporate (assuming that the snow surface is at 0°C) by the amount

$$EVAP = \frac{\Delta t_{phy}\ QFC1\ (q_{LM}-q_{sfc})}{\rho_w L_s \ APE_{sfc}} \qquad (125)$$

where L_s is the latent heat of sublimation. The snow depth (SNO) stored in meters of water is updated with the effects of melting and evaporation. After the update, if the snow depth is less than half of the amount lost to melting, the depth is set to zero.

Falling precipitation is added to SNO if it occurs over a land point and the surface temperature is at or below freezing otherwise it is considered to be rain. Evaporation of water over land is identical to that given in (125) except L_v replaces L_s. The soil moisture (WET) can now be updated by summing the rain, evaporation, and snow melt and is constrained to lie between 0 and 0.1125 m (WFC).

Clearly, an initial θ_{sfc} is needed before any surface calculations are done and is obtained from an adiabatic extrapolation from level LM:

$$\theta^0_{sfc} = T^0_{LM}\left(1+.608 q^0_{LM}\right)\ APE^0_{LM} \qquad (126)$$

Before being used in the integration, θ^0_{sfc} is smoothed:

$$\theta^0_{sfc}(new) = \theta^0_{sfc}(old) + .125\ \left\{\delta_x\cdot\left[\delta_x\cdot\theta^0_{sfc}(old)\right]+\delta_y\cdot\left[\delta_y\cdot\theta^0_{sfc}(old)\right]\right\} \qquad (127)$$

The underground temperature is similarly smoothed at this time.

4.4 Radiation

The routines which simulate the effects of radiation are essentially identical to those in the Nested Grid Model and are taken from those developed for the GLA GCM (Davies, 1982; Harshvardhan and Corsetti, 1984). Both shortwave and longwave interactions are described. Currently, the routines are called every Δt_{rad} =2 hrs during model integration.

Since the routines were created for sigma coordinate models, they must be passed vertical columns containing all model levels. However, due to the eta model's step-mountain structure, vertical columns may possess lower levels which are underground. To circumvent this obstacle, the vertical indices for each column are essentially "lifted" where necessary so that level LMAX becomes the lowest level over the ground. Any layers which are lifted above the top of the domain are isothermal to the true level 1, have specific humidities of 2×10^{-12}, and pressure depths of 100 Pa.

The amount of cloud in each layer (OCR) is a fraction between 0 and 1 and is found from the relation

$$OCR = 25\ \left(RH_L - RHCR\right)^2 \qquad (128)$$

where RHCR is 0.8. RH is the relative humidity in layer L but is bounded by 0.8 and 1.0. If OCR is less than 0.6, it is set to zero. Clouds are not allowed in the top four model layers or in the lowest one above ground.

The so-called skin temperature and air temperature at the ground are also needed. The former is taken from Eq.(121) while the latter is the temperature at a height of 2 m and is interpolated between the surface value and that at the lowest model level above ground using the logarithmic profile (see Eq.(84)).

In order to determine the intensity of the insolation, the cosine of the solar zenith angle is needed at all points (see Appendix).

Both the shortwave and longwave portions of the routine return atmospheric temperature tendencies in each level as well as the total downward flux. The tendencies (TEND) are summed and smoothed vertically by twice applying the relation

$$TEND_L = 0.5\left[TEND_L + \frac{TEND_{L-1}\ (\Delta\eta)_{L-1} + TEND_{L+1}\ (\Delta\eta)_{L+1}}{2\ (\Delta\eta)_L}\right] \qquad (129)$$

except at the uppermost level and lowest level above the ground. Next the tendencies are smoothed horizontally four times by applying the relation

$$TEND_L = TEND_L + .125\left[\delta_x^2\left(TEND_L\right) + \delta_y^2\left(TEND_L\right)\right] \qquad (130)$$

The total downward flux $R\downarrow$ is also smoothed horizontally four times using (130). The temperature tendencies are applied every Δt_{adj} during model integration while $R\downarrow$ is used in (121) to determine the surface temperature.

---------, -------, and S. Nickovic, D. Gavrilov, and D.G. Deaven, 1988: The step-mountain coordinate: Model description and performance for cases of Alpine lee cyclogenesis and for a case of Appalachian redevelopment. Accepted for publication, Mon. Wea. Rev.

Nickerson, E.C., and V.E. Smiley, 1975: Surface energy budget parameterizations for urban scale models. J. Appl. Meteor., 14, 297-300.

Phillips, N.A., 1957: A coordinate system having some special advantages for numerical forecasting. J. Meteor. 14, 184-185.

----------, 1974: Application of Arakawa's energy-conserving layer model to operational numerical weather prediction. NMC Office Note 104, 40pp. (NOAA, National Meteorological Center, WWBG, Room 101, Washington, D.C., 20233.)

Winninghoff, F.J., 1968: On the adjustment toward a geostrophic balance in a simple primitive equation model with application to the problems of initialization and objective analysis. Ph.D. thesis , Dept. of Meteorology, Univ. of California, Los Angeles, CA. 90024.

8 Appendix Calculation of the Solar Zenith Angle

At each call of the radiation routines, the location of the sun used is that at which it will be $\Delta t_{rad}/2$ into the future. First the celestial longitude of the sun (λ_s) is found from

$$\lambda_S = CLON1 + CLON2 \ DAY \ .$$

The constants CLON1 and CLON2 will vary each year but are approximately 279° and $0^{\circ}.99$, respectively. Precise values are taken from the Astronomical Almanac for the given year. DAY is the exact number of days from the beginning of the year to the pertinent forecast time. The solar declination δ_s and right ascension α_s are then

$$\delta_S = \sin^{-1}\left\{\sin(\lambda_S)\ \sin(\omega_E)\right\} \qquad (A1a)$$

$$\alpha_S = \cos^{-1}\left\{\cos(\lambda_S)/\cos(\delta_S)\right\} \qquad (A1b)$$

where ω_E - $23^{\circ}.441$ is the obliquity of the ecliptic.

Greenwich sidereal time is now found from

$$GST = CSID1 + CSID2 \ \ DAYI + CSID3 \ \ HOUR$$

where DAYI is the integral number of days from the beginning of the year to forecast time and HOUR is the exact number of hours on day DAYI+1 to the forecast time. Values of CSID1, CSID2, and CSID3 again vary from year to year and are taken from the Astronomical Almanac. The local solar hour angle at each grid point is $h = GST - \alpha_s - \lambda$, where λ is the geodetic longitude and GST is in angular form ($15^{\circ} = 1hr$). The cosine of the solar zenith angle ζ is then

$$\cos(\zeta) = \sin(\delta_S)\sin(\phi) + \cos(\delta_S)\cos(h)\cos(\phi) \qquad (A2)$$

where ϕ is the geodetic latitude.

Radiation Parameterization (GFDL) in NMC's Medium-Range Forecast Model (1992)

	Spectral region	Process	Comment
Clear sky	Longwave	Gas absorption	0 – 2200 cm^{-1} region
		H_2O	Hybrid scheme which separates the exchange between layers and the cooling to space (CTS) term in the radiative flux divergence equation (Schwarzkopf and Fels, 1991). The CTS term is calculated by a band model method using narrow bands (10 cm^{-1}) combined into 8 bands over the 160–560 cm^{-1} region. The exchange term is calculated using an emissivity formulation over wide band widths.
		H_2O continuum	Extended region, 400–1200 cm^{-1} (see Schwarzkopf and Fels, 1991 and Roberts *etal*, 1976).
		CO_2 and H_2O	CO_2 transmission based on pretabulated transmission functions for the 560–800 cm^{-1} region, with 2 bands used in CTS calculations (see Schwarzkopf and Fels, 1991 and 1985), where $CO_2 = 330$ ppmv.
		O_3	One interval random band model (Rodgers, 1968), where O_3 = seasonal zonal mean.
	Shortwave	Gas absorption	12 subintervals covering the solar spectrum
		O_3	Analytic formula of Lacis and Hansen (1974)
		H_2O	Subinterval structure of Lacis and Hansen (1974) formulation, modified from 8 to 12 bands at GFDL.
		CO_2	Formula of Sasamori *etal*, 1972
		Rayleigh scattering	Effects on O_3 as in Lacis and Hansen, 1974
		Diurnal cycle	Radiative flux calculation every 3 hours using daylight mean cosine of solar zenith angle over the time-interval...values then weighted by actual cosine zenith angle at each model point and time-step.
		Surface albedo	Land: Background from SiB climatology (Dorman and Sellers, 1989) which is altered in the presence of snow.....Open water: zenith angle dependent (Payne, 1972).....Sea ice : fixed background (= 0.5), altered by presence of snow.
Cloudy sky		Cloud overlap	Random
	Longwave	Scattering	None
		Absorption	Low, Middle cloud assumed black (emissivity = 1.0); while High cloud emissivity latitudinally dependent, varying between 0.6 in tropics and 0.3 at the poles.
	Shortwave	Scattering	Preset albedo for Low, Middle, High cloud
		Absorption	Preset absorption for Low, Middle, High cloud
		Multiple reflections	Between cloud layers, and between cloud base and earth's surface.

Radiation Parameterization used in NMC 's models

by K. A. Campana–14 Jan 92

Since NMC began making medium–range forecasts during the mid–1980's, we have had a close relationship with the radiation scientists at GFDL; specifically S. Fels, M. D. Schwarzkopf, and (recently) V. Ramaswamy. We have benefitted, over the years, from improvements that GFDL has made to their radiation schemes. The latest longwave (LW) scheme was implemented in the global model in February 1990, while a slightly updated shortwave (SW) scheme will be implemented in Winter 1991–92 . Currently, radiation calculations are made every 12 (model) hours, approximating the diurnal cycle via a cosine solar zenith angle weighting at each model time–step; however, with the above–mentioned model change, they will be made every 3 hours. The attached table reflects the NMC radiation scheme which will be operational later this winter. References for the table are listed below :

Dorman, J. L. and P. J. Sellers, 1989 : A global climatology of albedo, roughness length and stomatal resistance for atmospheric general circulation models as represented by the simple biosphere model (SiB), *J. of Appl. Meteor.*, 28, pp 833–855.

Lacis, A. A. and J. E. Hansen, 1974 : A parameterization for the absorption of solar radiation in the earth's atmosphere, *J. of Atmos. Sci.*, pp 118–133.

Payne, R. E., 1972 : Albedo of the sea surface, *J. of Atmos. Sci.*, pp 959–970.

Roberts, R., J. Selby, and L. Biberman, 1976 : Infrared continuum absorption by atmospheric water vapor in the 8–12 μ window, *Applied Optics*, pp 2085–2090.

Rodgers, C. D., 1968 : Some extensions and applications of the new random model for molecular band transmission, *Quart. J. of Roy. Meteor. Soc.*, pp 99–102.

Sasamori, T., J. London, and D. Hoyt, 1972 : *Radiation budget of the southern hemisphere, Meteorological Monographs*, 13, number 35, pp 9–23.

Schwarzkopf, M. D., and S. B. Fels, 1985 : Improvements to the algorithm for computing CO_2 transmissivities and cooling rates, *J. of Geophys. Res.*, pp 10541–10550.

Schwarzkopf, M. D., and S. B. Fels, 1991 : The simplified exchange method revisited: An accurate, rapid method for computation of infrared cooling rates and fluxes, *J. of Geophys. Res.*, 96, D5, pp 9075–9096.